Removal of cadmium and lead ions from aqueous solutions by novel dolomite-quartz@Fe3O4 nanocomposite fabricated as nanoadsorbent

Abdelaziz El Mouden, Noureddine El Messaoudi, Abdelqader El Guerraf, Amal Bouich, Valbonë Mehmeti, Abdellah Lacherai, Amane Jada, Juliana Heloisa Pinê Américo-Pinheiro

Removal of cadmium and lead ions from aqueous solutions by novel dolomite-quartz@Fe_3O_4 nanocomposite fabricated as nanoadsorbent

Abdelaziz El Mouden [a], Noureddine El Messaoudi [a,*], Abdelqader El Guerraf [b]
Amal Bouich [c], Valbonë Mehmeti [d], Abdellah Lacherai [a,*],
Amane Jada [e], Juliana Heloisa Pinê Américo-Pinheiro [f,g]

[a] *Laboratory of Applied Chemistry and Environment, Ibn Zohr University, Agadir 80000, Morocco*

[b] *Laboratory of Applied Chemistry and Environment, Faculty of Sciences, Mohammed First University, Oujda 60000, Morocco.*

[c] *Department of Applied Physics, Institute of Design and Manufacturing (IDF), Polytechnic University of Valencia, Valencia 46000, Spain*

[d] *Faculty of Agriculture and Veterinary, University of Prishtina, Prishtina10000, Kosovo*

[e] *Institute of Materials Science of Mulhouse (IS2M), High Alsace University, Mulhouse 68100, France*

[f] *Department of Forest Science, Soils and Environment, School of Agronomic Sciences, São Paulo State University (UNESP), Ave. Universitária, 3780, Botucatu - SP, 18610-034, Brazil*

[g] *Graduate Program in Environmental Sciences, Brazil University, Street Carolina Fonseca, 584, São Paulo - SP, 08230-030, Brazil*

*Corresponding authors:

Dr. Noureddine El Messaoudi: noureddine.elmessaoudi@edu.uiz.ac.ma

Dr. Abdellah Lacherai: a.lachera@uiz.ac.ma

Abstract

The elimination of heavy metal ion contaminants from residual waters is critical to protect humans and the environment. The natural clay (dolomite and quartz) based composite Fe_3O_4 nanoparticles (DQ@Fe_3O_4) has been largely explored for this purpose. Experimental variables such as temperature, pH, heavy metal concentration, DQ@Fe_3O_4 dose, and contact time were optimized in detail. The DQ@Fe_3O_4 nanocomposite was found to achieve a maximum of 95.02% for Pb^{2+} and 86.89% for Cd^{2+} removal at optimal conditions: pH of 8.5, adsorbent dose of 2.8 g L^{-1}, the temperature of 25 °C, and contact time of 140 min for 150 mg L^{-1} heavy metal ion concentration. The Co-precipitation of dolomite-quartz by Fe_3O_4 nanoparticles was justified by SEM-EDS, TEM, AFM, FTIR, XRD, and TGA analyses. The adsorption kinetics and equilibrium of the composite revealed that it fit the pseudo-second-order kinetic and Langmuir isotherm models as they both describe the best binding behavior of DQ@Fe_3O_4. This suggested a homogenous monolayer sorption dominated by surface complexation. Additionally, thermodynamic data have shown that the adsorption of heavy metal ions is considered a spontaneous and exothermic process. Moreover, Monte Carlo (MC) simulations were performed in order to clearly illuminate the interactions between heavy metal ions and the DQ@Fe_3O_4 nanocomposite surface. The results correlated well with experimental data and based on the negative values of the adsorption energy (Eads), the process of adsorption was confirmed to be spontaneous. In summary, the as-prepared DQ@Fe_3O_4 can be considered a low-cost-effective heavy metals adsorbent that has great potential in water treatment.

Keywords: Heavy metals ions, adsorption; dolomite-quartz; magnetite (Fe_3O_4) nanoparticles; Monte Carlo simulations; wastewater treatment

1 Introduction

In recent decades, the scientific community has increased the focus on minimizing the environmental issues caused by numerous organic and inorganic pollutants (El Messaoudi et al., 2022b; Esvandi et al., 2019; Foroutan et al., 2022b, 2018; Peighambardoust et al., 2021). Among the latter, heavy metal ions have gained vital consideration due to their high environmental persistence and toxicity. They are produced in wastewater from different industries, including metal plating, battery, dyeing, mining, and fertilizer industries, and then carried to rivers, lakes, and agricultural lands, where they infiltrate into living things and the human food chain. It has been established that harmful metals can enter the body of humans through food chains. Their accumulation has been associated with the onset of a number of diseases and conditions, including neurological disorders, different cancers, hormonal imbalances, malformation in fetuses, obesity, abortion, respiratory problems, infertility, and death (Balali-Mood et al., 2021; Espart et al., 2018; Foroutan et al., 2021a; Mitra et al., 2022; Munir et al., 2021). As such contaminants can pose grave threats to human health, animals, and plants as well as aquatic life even at low concentrations, it is necessary to find solutions that can lead to their removal before discharging into the environment.

The World Health Organization (WHO) and the International Program on Chemicals (IPCS) both classify the elements cadmium, zinc, copper, lead, nickel, mercury, arsenic, cobalt, and chromium as hazardous heavy metals (Peighambardoust et al., 2021). In particular, Cd and Pb have been considered primary contributors to the contamination of groundwater resources and excessive amounts can cause high blood pressure, cancer, as well as severe damage to the liver, kidney, hepatitis, bone, and nervous system (Zhang et al., 2021). It is reported that the maximum allowable concentrations in drinking water are 10 and 50 μg L^{-1} for lead and cadmium respectively.

Various physicochemical methods can be followed to decontaminate aqueous environments from toxic heavy metal ions (Srivastava and Majumder, 2008). With the help of chemical or electrochemical precipitation, membrane separation, reverse osmosis, ultrafiltration, flocculation/flotation, ion exchange, and sorption it is possible to eliminate these pollutants from aquatic solutions (Foroutan et al., 2022a, 2022b; Messaoudi et al., 2022; Shrestha et al., 2021). The majority of these approaches have limitations such as poor efficiency, high energy consumption, secondary sludge production, and also low sensitivity, especially with low concentrations of heavy metals which prevented their large-scale industrial application. In comparison with all known techniques, surface adsorption is the most preferred one for the treatment of wastewater, thanks to its high efficiency, low process cost, environmental friendliness, and considered flexible procedure (El Khomri et al., 2021; El Messaoudi et al., 2022c; Foroutan et al., 2020). In such a method, the choice of adsorbents is very important; the selected material should not cause secondary pollution in order to be more operational in nature (Dai et al., 2019). For this reason, it is vital to choose natural materials that are eco-friendly, recyclable, affordable, and have a large surface area and precursors (El Khomri et al., 2022b; El Messaoudi et al., 2021).

Various natural clays such as kaolinite, bentonite, montmorillonite, dolomite, and quartz are reported in the literature (Ahmadi et al., 2022; Polidori, 2007). These clays have attracted attention due to their abundance in nature, cost-effectiveness, high removal capacity, and ability to be reused several times for water purification**.** Natural clays are sustainable mineral environmentally friendly materials (Ashour and Tony, 2020) that contain many groups (Ashour and Tony, 2020) responsible for the interaction with inorganic pollutants through hydrogen bonding and complexation (Khan and Khan, 2021). Therefore, this study focused on using such environmentally friendly adsorbent for the elimination of toxic metal ions from wastewater. Nowadays, the valorization of nanotechnology of sourced materials such as nanocomposites which are currently being studied is becoming more and more interesting for

scientific researchers due to their low toxicity, paramagnetic, and small size (Almahri, 2022; Szabó et al., 2007). Therefore, natural clay is considered to be one of the most promising candidates to prepare nanocomposites. With the co-precipitation of Fe_3O_4 nanoparticles in the natural clay matrix, the morphological structure of the natural clay can be significantly affected which generates a highly efficient adsorbent (El-Naggar et al., 2021). Fe_3O_4-based nanomaterials have been used as effective adsorbents due to their unique characteristics such as small particle size, high specific surface area, and also superparamagnetic properties (Abdollahi et al., 2021).

This is the framework in which our paper fits. A high-performance adsorbent based on natural clay [constituted from dolomite CaMg $(Co_3)_2$) and quartz (SiO_2 + Al_2O_3)] and Fe_3O_4 nanoparticles were developed by the co-precipitation method. The newly synthesized dolomite-quartz@Fe_3O_4 (DQ@Fe_3O_4) nanocomposite was analyzed by numerous microscopic and spectroscopic techniques, then used to eliminate Pb^{2+} and Cd^{2+} ions from water. The adsorption data were estimated by means of different kinetic and isothermal models and thermodynamic parameters. In addition, the adsorption process on DQ@Fe_3O_4 has been investigated with Monte Carlo (MC) simulation method, and the adsorption energy, as well as the geometry of heavy metal-DQ@Fe_3O_4 nanocomposite surface were discussed.

2 Materials and methods

2.1. Chemicals

Iron (III) chloride hexahydrate ($FeCl_3 \cdot 6H_2O$, ≥98.0%), iron (II) sulfate heptahydrate ($FeSO_4 \cdot 7H_2O$, ≥99.0%), and ammonium hydroxide solution (NH_4OH, 99.9%) were purchased from Fluka. Lead (II) nitrate ($Pb(NO_3)_2$, ≥99.0%), cadmium (II) Nitrate Tetrahydrate ($Cd(NO_3)_2 \cdot 4H_2O$, 99.9%), hydrochloric acid (HCl, 37%), and sodium hydroxide (NaOH, 98%) were supplied by Sigma-Aldrich. Reagents were used as received and all practical solutions were prepared with bi-distilled water.

2.2 Synthesis of the DQ@Fe_3O_4 nanoadsorbent

Fe_3O_4 NPs were synthesized by a mixture of $FeCl_3 \cdot 6H_2O$ (2.3348 g, 8.6 mmol) and $FeSO_4 \cdot 7H_2O$ (1.2008 g, 4.3 mmol) dissolved into 100 ml of deionized water (molar ratio of Fe(III): Fe(II)=2:1). NH_4OH solution (100 ml, 5 M) is added dropwise to precipitate the iron oxides. The obtained Fe_3O_4 NPs (**Eq. (1)**) were magnetically separated and washed with distilled water and C_2H_5OH, respectively.

$$FeSO_4 + 2\ FeCl_3 + 8\ NH_4OH \rightarrow Fe_3O_4 + 6\ NH_4Cl + (NH_4) \qquad \text{Eq. (1)}$$

DQ@Fe_3O_4 were elaborated according to the Massart co-precipitation process (Liu et al., 2020), Briefly, 1g of Fe_3O_4 NPs was mixed with 2 g dolomite-quartz and dissolved in 100 mL of aqueous solution at 70°C. The reaction was kept for 6 h.

2.3 Characterization of the adsorbent

The structural features of DQ@Fe_3O_4 nanocomposite were characterized by Fourier transform infrared spectroscopy (FTIR, Iraffinity 1S Shimadzu), X-ray diffraction (XRD, Bruker D8), and thermogravimetric analyzer Shimadzu DTG-60/60 was used to assess the material's thermal stability. On the other hand, the morphological characterization was carried out using scanning electron microscopy/energy-dispersive X-ray spectrometry (SEM-EDS) model JEOL JSM IT-100, transmission electron microscopy (TEM, JEM2100F), as well as atomic force microscopy (AFM) with a Bruker Multimode 8 instrument.

2.4 Batch adsorption experiments

The influence of operating conditions, including the initial pH (2.5–10), contact time (20–200 min), and the initial concentration of heavy metals (50–350 mg L^{-1}) using 0.2–4 g L^{-1} of DQ@Fe_3O_4 at a temperature range of 25–45°C were studied to evaluate the performance of DQ@Fe_3O_4. At the end of the adsorption reaction, adsorbent and adsorbate were separated by using a 0.22 μm filter (Millex). An atomic absorption spectrometer (AAS; PinAAcleTM 500) was used for the determination of Pb^{2+} and Cd^{2+} ions in the solution. The removal percentage

and amount of metal ions adsorbed at equilibrium q_e (mg g^{-1}) were calculated using **Eqs. (2)** and **(3)**, respectively.

$$\% \, Removal = \frac{(C_i - C_f)}{C_i} \times 100 \qquad \text{Eq. (2)}$$

$$q_e = \frac{(C_i - C_f) \times V}{m} \qquad \text{Eq. (3)}$$

With m(g) is the amount of DQ@Fe_3O_4, C_i (mg L^{-1}) and C_f (mg L^{-1}) are the initial and final heavy metal concentrations, and V(L) represents the volume of the solution.

2.5 Computational calculations

The interaction between heavy metal ions and the modeled co-precipitated surfaces of natural clay [dolomite ($CaMg(Co_3)_2$) and quartz ($SiO_2 + Al_2O_3$)] is studied using Monte Carlo (MC) simulations. The calculations were constructed using Layer Builder in the Biovia software, both surface types were expanded using 4x4 cell units, combined and then a 35 Å vacuum layer was added to accommodate metal ions and 700 water molecules. The universal force field (UFF) was used for the simulation calculations (Khalaf et al., 2021; Rappé et al., 1992; Ulusoy et al., 2022).

3 Results and discussion

3.1 Characterization of the DQ@Fe_3O_4 nanocomposite

Firstly, FTIR analysis was achieved for bare natural clay, Fe_3O_4, and the synthesized adsorbent DQ@Fe_3O_4. As shown in **Fig. 1a**, DQ@Fe_3O_4 before adsorption has several specific peaks that characterize some mineral phases. The band at 1046 cm^{-1} and 462 cm^{-1} describe the silica phase and correspond to the stretching vibration of Si-O and Si-O-Si (Bentahar et al., 2017). The bands at around 1436 cm^{-1}, 878 cm^{-1}, and 789 cm^{-1} are due to CO_3^{2-} groups in the dolomite structure (Correia et al., 2015; Ji et al., 2009). The absorption peaks located at 3639 cm^{-1} and 1631 cm^{-1} are attributed to the vibration of the O-H hydroxyl group and the deformation of the H_2O molecules (Bentahar et al., 2017; Mohankumar et al.,

2021). In the case of the synthesized magnetite powder Fe_3O_4, four characteristic bands appear in the spectrum. The main absorption peaks at 541 cm^{-1} and 431 cm^{-1} correspond to the intrinsic stretching vibration of the Fe–O bonds at tetrahedral and octahedral sites in the crystalline Fe_3O_4, respectively (Asab et al., 2020; Foroutan et al., 2021b; Yang et al., 2018). The broad band at 3408 cm^{-1} and the other one observed at 1631 cm^{-1} represent the stretching vibrations of O-H hydroxyl groups (Yang et al., 2010). It is thus confirmed that during the elaboration of iron oxide in an aqueous medium, the surface was covered with hydroxyl groups of water. On the other hand, the spectra of the composite DQ@Fe_3O_4 have clearly shown the integration of the magnetic nanoparticles into the dolomite-quartz. As can be seen, the intense peaks associated with silica (1046 cm^{-1}) and dolomites (789 cm^{-1}) are present in the spectra of the composite. Additionally, the spectrum of the DQ@Fe_3O_4 displays bands in the region of 400–570 cm^{-1} which characterize the Fe–O vibration. Hence, the FTIR investigation has confirmed the formation of the composite based on the dolomite-quartz material and magnetic nanoparticles.

Furthermore, chemically synthesized dolomite-quartz, Fe_3O_4, and DQ@Fe_3O_4 have also been characterized by XRD, and all spectra are shown in **Fig. 1b**. The diffractogram of dolomite-quartz has demonstrated the presence of numerous reflections which indicate the existence of various phases. The peaks at 2θ=21.80°, 24.12°, 30.90°, 33.50°, 37.40°, 41.10°, 44.80°, 50.60°, 51.00°, and 60.00° correspond to the Miller indices: (101), (012), (104), (006), (110), (113), (202), (018), (116), and (211) of dolomite (JCPDS N°. 36–0426) (Bentahar et al., 2017; Qiu et al., 2015). The reflections at 2θ=26.6°, 35.9°, and 50.20° belong to the plans (101), (110), and (112) of silica SiO_2 which is in good agreement with standards JCPDS N° 33–1161 (Bentahar et al., 2017). In addition, the XRD patterns display also a minority phase corresponding to alumina Al_2O_3. Indeed, the reflections that appeared at Bragg angles of 42.40°, 43.90°, and 56.60° are attributed to the presence of the rhombohedral system α-Al_2O_3 referenced in the JCPDS file N° 71–1123 (Mohankumar et al., 2021). Further analysis will be

carried out with EDS spectroscopy to strengthen this discussion. In the case of the synthesized nanoparticles, the XRD spectrum of magnetite Fe_3O_4 has shown several peaks at 18.45°, 30.29°, 35.64°, 43.25°, 53.58, 57.20°, and 62.81° assigned to the plans (111), (220), (311), (400), (422), (511) and (440), respectively. This is in line with the typical pattern JCPDS N° 79–0417 for Fe_3O_4 (Asab et al., 2020; Jamshidiyan et al., 2017; Malega et al., 2018). It should be noted that the elaborated magnetic nanoparticles Fe_3O_4 have demonstrated very broad peaks, which suggest the ultra-fine nature and small crystallite size of the particles. The phase identification by XRD spectroscopy was also achieved for the DQ@Fe_3O_4. As shown, the XRD patterns of the composite have demonstrated the presence of all peaks related to the clay phase. In addition, the 2θ reflections of Fe_3O_4 nanoparticles are also seen. Thus, the successful modification of the dolomite-quartz is confirmed.

The thermal characteristics of DQ, Fe_3O_4, and DQ@Fe_3O_4 were then analyzed by TGA (**Fig. 1c**). In the case of magnetite Fe_3O_4, two mass losses were observed. The first peak occurs between 30 and 150 °C, which are close to the point at which water molecules that have been absorbed may evaporate. While the second degradation in the range 230-700°C, where the percentage of mass loss is about 2%, is attributed to the phase transition from magnetite to hematite (Massaro et al., 2021; Wan Fatihah Khairunisa Wan Nor et al., 2018).

The TGA curve obtained for DQ shows also two major mass losses between 20-150°C and 400-700°C. The initial weight loss is associated with the evaporation of surface-adsorbed water molecules in the intercalated space (Bentahar et al., 2019; Wang et al., 2021) and the second stage, with a weight loss rate of approximately 6%, is due to the degradation of silica, dolomite, and alumina (Bernal et al., 2017). Furthermore, the TG analysis of the DQ@Fe_3O_4 nanomaterial exhibited a similar decomposition pattern as the natural clay with, however, superior thermal stability compared to unmodified dolomite-quartz in the examined temperature range.

On the other hand, SEM micrographs as well as the EDS spectra of DQ and DQ@Fe_3O_4 are presented in **Fig. 2**. As shown, dolomite-quartz is characterized by a partially uniform morphology constituted by homogeneously dispersed microspherical grains with different sizes ranging between 3 and 10 µm (**Fig. 2a** and **b)** (Bentahar et al., 2016). The corresponding EDS spectra (**Fig. 2c**), indicate the presence of carbon, oxygen, magnesium, aluminum, silicon, and calcium, which suggest that the analyzed material is constituted of dolomite, silica as well as alumina (Bentahar et al., 2017). The SEM analysis of the modified dolomite-quartz has demonstrated no significant change in the morphology. It is clear that for DQ@Fe_3O_4 **Fig. 2d**, and **e**, the spherical geometry of the dolomite-quartz based material is retained with the presence of a thin layer that covers the dolomite-quartz surface. On the other hand, the EDS spectra have clearly shown the presence of Fe (**Fig. 2f)** which indicates the successful modification of the natural material. The topographic and elemental analysis have also been carried out for the DQ@Fe_3O_4 composite after the adsorption process of Pb^{2+} and Cd^{2+} ions (**Fig. 2g** and **h**). A slight modification in the morphology of DQ@Fe_3O_4 has been observed after the interaction with the metallic ions. Moreover, the chemical analysis has clearly demonstrated the presence, besides the elements originating from the composite, other ones resulting from the interaction with the heavy metal ions. Indeed, the EDS spectra of **Fig. 2** indicate the presence of lead and cadmium for the composite, which confirms the successful integration of Pb^{2+} and Cd^{2+} into the adsorbent matrix. Additionally, the EDS elemental mapping, shown in the same figure, evidenced a uniform and homogenous distribution of these elements in the synthesized composite. The SEM-EDS characterization of DQ@Fe_3O_4 after the adsorption has been achieved to demonstrate the capacity of these compounds to adsorb heavy metal ions. Hence, this preliminary study has allowed us to better perform a detailed analysis of the adsorption process.

Afterward, in order to better comprehend the particle size distribution, the synthesized DQ@Fe_3O_4 nanoparticles were further analyzed by HRTEM. From the image of **Fig. 3a** and

b, lattice fringe spacings of about 0.26 nm were measured for the DQ@Fe_3O_4, this is in good agreement with the d-spacing of the (311) plane in cubic Fe_3O_4 nanocrystals (0.25 nm) obtained from the XRD data (Liu et al., 2015; Xu et al., 2015). Moreover, the selected area electron diffraction (SAED) pattern presented in **Fig. 3c** has a highly symmetrical dotted lattice, exhibiting the polycrystalline nature of the Fe_3O_4. The particle size distribution of the DQ@Fe_3O_4 was also calculated (**Fig. 3d**) and was found at about 21.40 nm. **Fig. 3e** and **f** present the AFM images of the material in 2 and 3 dimensions. It is shown the good homogeneity of DQ@Fe_3O_4 grain size and the root-mean-square (RMS) was found equal to 58.4 nm. The morphology is correlated to alloys until a certain point with high roughness.

3.2 Effects of adsorbent dose and pH

As necessary factors in the adsorption process, the adsorbent dose is always studied and it is considered an important criterion that can affect the behavior of the adsorbent toward the pollutants. Only with optimum dose, the efficiency can be at maximum. **Fig. 4a** shows the effect of the DQ@Fe_3O_4 dose on the adsorption of lead and cadmium ions. It is noticed that the elimination capacity of Pb^{2+} and Cd^{2+} ions increased from 31.8 to 97.50% and 13.0 to 91.01%, respectively. The uptake efficiency increases with the increase in the adsorbent dose up to 2.8 g L^{-1} for DQ@Fe_3O_4. This increase is due to the accessibility of the adsorption sites and the large specific surface (Burham and Sayed, 2016; Dinh et al., 2022). With a dose beyond 2.8 g L^{-1}, the uptake efficiency is stable and the increase of the adsorbent concentration does not affect the uptake process which can be explained by the saturation of the DQ@Fe_3O_4 nanocomposite surface (Es-said et al., 2021).

Additionally, the pH is also seen as a crucial parameter that needs to be discussed (Jiang et al., 2020). Depending on the degree of the electrostatic charge, different amounts of metal ions from the wastewater are transmitted to the adsorbent (Yeow et al., 2021). A parameter like pH can control the movement of the electrostatic charges and cause their change on the surface of the adsorbent DQ@Fe_3O_4. Firstly, the pH at which the net adsorbent surface charge is zero

was determined by measuring the pH point of zero charges (pH_{pzc}). Generally, on the basis of pH_{PZC}, where the adsorbent surface is neutral, it is possible to explain the influence of pH on the adsorption process of metal ions. The zero load point of the DQ@Fe_3O_4 was found to be PZC = 6 (**Fig. 4c**). This means that when the pH is below 6, the surface of DQ@Fe_3O_4 has a positive charge, and at a pH above 6, negatives charges dominate on the surface (Zyoud et al., 2019). The influence of pH on Pb^{2+} and Cd^{2+} adsorption to DQ@Fe_3O_4 was examined in the pH range of 2.5–10, (**Fig. 4b)**. The investigation was achieved with 2.8 g L^{-1} of DQ@Fe_3O_4 dose at $25 \pm 1°C$. The uptake efficiency increases from 25.41 to 98.62% and from 23.52 to 91.78% for $Pb^{2+}$and Cd^{2+}, respectively. The removal rates on DQ@Fe_3O_4 were low at pH = 2.5 as a result of the competition of a small number of binding sites at low pH values between hydrogen and metal ions. In addition, studies have shown that in the range of pH < 7 the Fe ions will not be generated in the system (Yang et al., 2022). Hence, we can draw the conclusion that metal ions' adsorption capacity likewise rises with increasing pH value, showing that an electrostatic interaction occurs on the adsorbent's surface where negatively charged active sites are exposed to the solution (Van Tran et al., 2019) resulting in metal ions uptake. On the contrary, at lower pH values, electrostatic repulsions of positively charged functional groups from the DQ@Fe_3O_4 surface will eventually decrease the adsorption rate. In a conclusion, a pH of 8.5 was selected as an optimum value for further analysis.

The dolomite-quartz may combine with Fe_3O_4 through the surface hydroxyl group and the intermediate oxygen (-O-) in the carboxyl functional group. The interaction is simplified in **Eq. (4)** (Tan et al., 2017).

$$R\text{-}OH + (Fe_3O_4) \rightarrow R\text{-}O\text{-}(Fe_3O_4) \qquad \text{Eq. (4)}$$

3.3 Adsorption kinetics

Pseudo-first order (PFO), pseudo-second order (PSO), intraparticle diffusion (IPD), and Elovich models are commonly used to explain adsorption kinetics. As a result of the fit to the models, the adsorption mechanism can be predicted. The assumptions, equations, and

parameters of the PFO, PSO, IPD, and Elovich models have been described in many studies in the literature (Afolabi et al., 2020; Castro et al., 2018; Sharma et al., 2019; Tan and Hameed, 2017).The kinetic modeling of Pb^{2+} and Cd^{2+} adsorption on DQ@Fe_3O_4 is presented in **Fig. 5. Table 1** shows the calculated parameters using the various kinetic models. It is seen that the R^2 values of the PSO model are as compared higher than the PFO, IPD, and Elovich models. Furthermore, as the experimental $q_{e,exp}$ values (61.96 mg g^{-1} and 58.08 mg g^{-1} for Pb^{2+} and Cd^{2+}, respectively) are practically similar to those obtained theoretically in the case of the PSO model (63.92 mg g^{-1} and 60.19 mg g^{-1} for Pb^{2+} and Cd^{2+}, respectively), we can assume that the heavy metals adsorption on DQ@Fe_3O_4 is well fitted the PSO model.

Regarding the IPD model fitting, it is noticed that it has two linear components instead of a single line passing through the origin. In this case, the adsorption processes include firstly rapid adsorption to the surface followed by relatively slow intraparticle diffusion steps. Thus, it is difficult to explain the adsorption process with a single kinetic model, and the adsorption kinetics of both metal ions onto DQ@Fe_3O_4 nanocomposite can only be explained by the PSO model.

3.4 Adsorption isotherms

In the following, experimental data were applied to different isotherms models namely, Langmuir, Freundlich, Temkin, and Dubinin-Radushkevic (**Fig. 6)**. The suitability of the models was evaluated by comparing the statistical data in **Table 2**. As demonstrated, the correlation coefficients for Pb^{2+} and Cd^{2+} of the Langmuir model (R^2 = 0.999) are larger than those of the Freundlich (0.908 for Pb^{2+} and 0.868 for Cd^{2+}), Temkin (0.981 for Pb^{2+} and 0.944 for Cd^{2+}), and Dubinin-Radushkevic (0.957 for Pb^{2+} and 0.907 for Cd^{2+}) adsorption isotherms. In addition, higher uptake capacity (Q_m) was obtained with the first model (71.68 mg g^{-1} and 68.49 mg g^{-1} for Pb^{2+} and Cd^{2+}, respectively). This confirms that the heavy metal adsorption data are best fitted to the Langmuir isotherm model. The latter presumes homogenous monolayer adsorption with equal affinities of active sites for adsorbate molecules (El

Messaoudi et al., 2022d). The calculated values of $R_L=1/(1+ K_LC_0)$ (0.023 for Pb^{+2} 0.058 for Cd^{+2}) are positive but less than one which indicates favorable adsorption (Rezaei Kalantry et al., 2015). The adsorption energy ($E=1/(2\ \beta)^{1/2}$) of DQ@Fe_3O_4 nanocomposite obtained from Dubinin-Radushkevich isotherm were 2.236 kJ mol^{-1} and 0.353 kJ mol^{-1} for Pb^{+2} and Cd^{+2}, respectively. These values less than 8 kJ mol^{-1} reflect the physical nature of the adsorption (Isiuku et al., 2021).

In order to describe the interesting adsorption capability of the elaborated nanomaterial, the maximal sorption capacities of Pb^{2+} and Cd^{2+} ions onto variously reported adsorbents compared to DQ@Fe_3O_4 are presented in **Table 3**. Several materials based on natural clay and magnetic nanoparticles were tested for their heavy metal uptake and as it appears, the prepared composite in the present work is highly efficient with a high adsorption capacity. The natural properties, recyclability as well as low cost of such adsorbent can further enhance its potential application in water industries.

3.5 Adsorption thermodynamic

To explain the thermodynamic behavior of Pb^{2+} and Cd^{2+} removal using DQ@Fe_3O_4, the temperature effect was studied in the range from 25 to 45°C. Thermodynamic parameters ΔH^0, ΔS^0, and ΔG^0 were calculated using the **Eqs. (5-7)** presented below (El Messaoudi et al., 2022a; Şimşek et al., 2017).

$$\Delta G° = -RTLnK_d \qquad \text{Eq. (5)}$$

$$LnK_d = \frac{\Delta S°}{R} - \frac{\Delta H°}{RT} \qquad \text{Eq. (6)}$$

$$K_d = \frac{(1000.K_g.\text{molecular weight of adsorbate}.[\text{adsorbate}]^0)}{\gamma} \qquad \text{Eq. (7)}$$

Here, R(8.314 J mol^{-1} K^{-1}) is the ideal gas constant, T (K) is the temperature, and K_d is the thermodynamic equilibrium constant (Chen et al., 2019; Lima et al., 2019). K_g is the best fitted isotherm model constant, γ is the coefficient of activity of the adsorbate (dimensionless)

and [adsorbate]^0 is the standard concentration of the adsorbate (1 mol L^{-1}). The effect of temperature on Pb^{2+} and Cd^{2+} adsorption to DQ@Fe_3O_4 was evaluated by plotting the lnK_d-1/T graph (**Fig. 7a**). Using the lnK_d-1/T linear relationship; ΔH^o and ΔS^o are calculated from the slope and cut off the line, respectively. The thermodynamics parameters were calculated and displayed in **Table 4**. The negative values of the ΔG^o indicate that the adsorption of Pb^{2+} and Cd^{2+} onto DQ@Fe_3O_4 was a spontaneous process (El Khomri et al., 2022a; Yang et al., 2017; Zhang et al., 2021).

Further, the negative value of ΔH^o demonstrates that the adsorption process is exothermic in nature (Duan et al., 2020; Lin et al., 2019). While the negative ΔS^o proves the decrease in the randomness of Pb^{2+} and Cd^{2+} adsorption on DQ@Fe_3O_4 (Haounati et al., 2021). Meaning that as the sorption process proceeded, the level of disorder at the adsorbent-metal solution interface decreased, thus, the system is stable and the internal structure of DQ@Fe_3O_4 is maintained.

3.6 Recyclability of DQ@Fe_3O_4 nanocomposite

One of the important properties of an adsorbent is the capability of reusing it several times in the uptake process. For this, a recyclability test was achieved. After subjecting DQ@Fe_3O_4 to an adsorption run at pH=8.5, the material was recycled to the following adsorption stage by removing the loaded Pb^{2+} and Cd^{2+} using NaOH (10 mL, 0.5 M). The removal efficiency of Pb^{2+} and Cd^{2+} ions on DQ@Fe_3O_4 as a function of a number of cycles is shown in **Fig. 7b**. At first contact of the synthesized adsorbent with the heavy metal ions, the removal efficiency is higher than 90%. After 5 repetitive cycles, the adsorption capacity decreased by approximately 5%. This decrease does not remarkably affect the high uptake properties of the material and it is considered normal as some metal ions can always penetrate throughout the pores and remain attached to the adsorbent (Khomri et al., 2022).

3.7 Monte Carlo investigations

The energies are based on adsorbate-adsorbent interactions. Find adsorption energy (Eads) was calculated using **Eq. (8)** (Guo et al., 2014; Hsissou et al., 2019).

$$E_{ads} = E_{Adsorbent\ Surface/\text{Metal ion}} - (E_{Adsorbent\ Surface} + E_{\text{Metal ion}}) \qquad \text{Eq. (8)}$$

Where, $E_{\text{Adsorbent surface/Metal}}$, $E_{\text{Adsorbent surface}}$, and $E_{\text{Metal ion}}$ represent the total energies of the adsorption system, the adsorbent, and the metal ion, respectively.

The binding of the Pb^{2+} and Cd^{2+} onto the surface of the DQ@Fe_3O_4 nanocomposite is performed via MC calculations. This method of measuring molecular intricacy uses random permutations of simulation box species (molecules, ions). The adsorption energy for the lead and cadmium ions on the modeled surfaces of dolomite-Fe_3O_4 and the quartz-Fe_3O_4 surface is presented in **Fig. 8**. E_{ads} was found as -481.85 kcal mol^{-1}, -640.64 kcal mol^{-1}, -622.05 kcal mol^{-1}, and -774.45 kcal mol^{-1} for Pb^{2+}-Fe_3O_4-dolomite, Pb^{2+}-Fe_3O_4-quartz, Cd^{2+}-Fe_3O_4-dolomite, and Cd^{2+}-Fe_3O_4-quartz, respectively. Based on these results, the binding of heavy metal ions on DQ@Fe_3O_4 is suggested to be spontaneous (Jafari et al., 2022). **Fig. 9** shows the geometry of the heavy metal ions on the modeled surfaces. The experimental findings are supported by a noticeably greater negative value of Eads of the adsorbate molecules onto the surface of the adsorbents. This conclusion may also be drawn from the study of the final geometrical pose of the MC, where it is evident that the metal ions are in close proximity to the surface (Chen et al., 2016; Nairat et al., 2022). The experimental finding lends more credibility to the notion that the metal ions (cadmium and lead) possess considerable negative adsorption energies (spontaneous adsorption).

4 Conclusions

Simple and low-cost synthesis of clay-based nanocomposite and its use as heavy metals adsorbent was fully discussed. The DQ@Fe_3O_4 material was elaborated by a co-precipitation method and was then characterized using several microscopic and spectroscopic techniques.

FTIR, XRD, TGA, SEM, and TEM analyses have demonstrated the successful integration of iron oxide nanoparticles onto the natural clay matrix. Afterward, Pb^{2+} and Cd^{2+} removal capacity was studied for the elaborated composite by varying several characteristic parameters including, pH, contact time, adsorbent dosage, and heavy metals concentration. Under optimal conditions of 8.5 pH, 2.8 g L^{-1} adsorbent dose, 150 mg L^{-1} metal ions concentration with a contact time of 140 min at 25°C, the quantity adsorbed was found to be around 71.42 mg g^{-1} and 68.49 mg g^{-1} for Pb^{2+} and Cd^{2+}, respectively. PSO kinetic and Langmuir isotherm models have well described the adsorption equilibrium of lead and cadmium ions on the DQ@Fe_3O_4 nanocomposite. In addition, the interaction adsorbent-adsorbate was discussed by Monte Carlo simulations and the results were correlated with experimental data. The synthesized DQ@Fe_3O_4 nanocomposite has proven high adsorption capacity for both ions which suggests its possible use for the treatment of industrial wastewater.

References

Abdollahi, H., Maleki, S., Sayahi, H., Gharabaghi, M., Darvanjooghi, M.H.K., Magdouli, S., Brar, S.K., 2021. Superadsorbent Fe3O4-coated carbon black nanocomposite for separation of light rare earth elements from aqueous solution: GMDH-based Neural Network and sensitivity analysis. J. Hazard. Mater. 416, 125655. https://doi.org/10.1016/J.JHAZMAT.2021.125655

Afolabi, I.C., Popoola, S.I., Bello, O.S., 2020. Modeling pseudo-second-order kinetics of orange peel-paracetamol adsorption process using artificial neural network. Chemom. Intell. Lab. Syst. 203, 104053. https://doi.org/10.1016/J.CHEMOLAB.2020.104053

Ahmadi, A., Foroutan, R., Esmaeili, H., Peighambardoust, S.J., Hemmati, S., Ramavandi, B., 2022. Montmorillonite clay/starch/CoFe2O4 nanocomposite as a superior functional material for uptake of cationic dye molecules from water and wastewater. Mater. Chem. Phys. 284, 126088. https://doi.org/10.1016/J.MATCHEMPHYS.2022.126088

Ahmaruzzaman, M., 2011. Industrial wastes as low-cost potential adsorbents for the treatment of wastewater laden with heavy metals. Adv. Colloid Interface Sci. 166, 36–59. https://doi.org/10.1016/J.CIS.2011.04.005

Almahri, A., 2022. The solid-state synthetic performance of bentonite stacked manganese ferrite nanoparticles: adsorption and photo-fenton degradation of MB dye and antibacterial applications. J. Mater. Res. Technol. 17, 2935–2949. https://doi.org/10.1016/J.JMRT.2022.02.052

Asab, G., Zereffa, E.A., Abdo Seghne, T., 2020. Synthesis of Silica-Coated Fe3O4 Nanoparticles by Microemulsion Method: Characterization and Evaluation of Antimicrobial Activity. Int. J. Biomater. 2020. https://doi.org/10.1155/2020/4783612

Ashour, E.A., Tony, M.A., 2020. Eco-friendly removal of hexavalent chromium from aqueous solution using natural clay mineral: activation and modification effects. SN Appl. Sci. 2, 1–13. https://doi.org/10.1007/S42452-020-03873-X/FIGURES/9

Badruddoza, A.Z.M., Shawon, Z.B.Z., Tay, W.J.D., Hidajat, K., Uddin, M.S., 2013. Fe3O4/cyclodextrin polymer nanocomposites for selective heavy metals removal from industrial wastewater. Carbohydr. Polym. 91, 322–332. https://doi.org/10.1016/J.CARBPOL.2012.08.030

Balali-Mood, M., Naseri, K., Tahergorabi, Z., Khazdair, M.R., Sadeghi, M., 2021. Toxic Mechanisms of Five Heavy Metals: Mercury, Lead, Chromium, Cadmium, and Arsenic. Front. Pharmacol. 12, 227. https://doi.org/10.3389/FPHAR.2021.643972/BIBTEX

Bentahar, S., Dbik, A., El, M., Bakiz, B., Lacherai, A., 2016. ORIGINAL RESEARCH PAPER STUDY OF REMOVAL OF CONGO RED BY LOCAL NATURAL CLAY 17, 295–307.

Bentahar, S., Dbik, A., Khomri, M. El, El Messaoudi, N., Lacherai, A., 2017. Adsorption of methylene blue, crystal violet and congo red from binary and ternary systems with natural clay: Kinetic, isotherm, and thermodynamic. J. Environ. Chem. Eng. 5, 5921–5932. https://doi.org/10.1016/J.JECE.2017.11.003

Bentahar, S., Taleb, M.A., Sabour, A., Dbik, A., El Khomri, M., El Messaoudi, N., Lacherai, A., Mamouni, R., 2019. Potassium Fluoride-Modified Clay as a Reusable Heterogeneous Catalyst for One-Pot Synthesis of 3,4-Dihydropyrimidin-2(1H)-ones. Russ. J. Org. Chem. 55, 1423–1431. https://doi.org/10.1134/S1070428019090240

Bernal, S.A., Juenger, M.C.G., Ke, X., Matthes, W., Lothenbach, B., De Belie, N., Provis, J.L., 2017. Characterization of supplementary cementitious materials by thermal analysis. Mater. Struct. Constr. 50. https://doi.org/10.1617/s11527-016-0909-2

Burham, N., Sayed, M., 2016. Adsorption behavior of Cd2+ and Zn2+ onto natural Egyptian bentonitic clay. Minerals 6. https://doi.org/10.3390/min6040129

Castro, L., Blázquez, M.L., González, F., Muñoz, J.A., Ballester, A., 2018. Heavy metal adsorption using biogenic iron compounds. Hydrometallurgy 179, 44–51. https://doi.org/10.1016/J.HYDROMET.2018.05.029

Chen, D., Zhang, H., Yang, K., Wang, H., 2016. Functionalization of 4-aminothiophenol and 3-aminopropyltriethoxysilane with graphene oxide for potential dye and copper removal. J. Hazard. Mater. 310, 179–187. https://doi.org/10.1016/j.jhazmat.2016.02.040

Chen, S., Qin, C., Wang, T., Chen, F., Li, X., Hou, H., Zhou, M., 2019. Study on the adsorption of dyestuffs with different properties by sludge-rice husk biochar: Adsorption capacity, isotherm, kinetic, thermodynamics and mechanism. J. Mol. Liq. 285, 62–74. https://doi.org/10.1016/J.MOLLIQ.2019.04.035

Correia, L.M., de Sousa Campelo, N., Novaes, D.S., Cavalcante, C.L., Cecilia, J.A., Rodríguez-Castellón, E., Vieira, R.S., 2015. Characterization and application of dolomite as catalytic precursor for canola and sunflower oils for biodiesel production. Chem. Eng. J. 269, 35–43. https://doi.org/10.1016/J.CEJ.2015.01.097

Dai, Y., Zhang, N., Xing, C., Cui, Q., Sun, Q., 2019. The adsorption, regeneration and engineering applications of biochar for removal organic pollutants: A review. Chemosphere 223, 12–27. https://doi.org/10.1016/J.CHEMOSPHERE.2019.01.161

Dinh, V.P., Nguyen, P.T., Tran, M.C., Luu, A.T., Hung, N.Q., Luu, T.T., Kiet, H.A.T., Mai, X.T., Luong, T.B., Nguyen, T.L., Ho, H.T.T., Nguyen, D.K., Pham, D.K., Hoang, A.Q., Le, V.T., Nguyen, T.C., 2022. HTDMA-modified bentonite clay for effective removal of Pb(II) from aqueous solution. Chemosphere 286. https://doi.org/10.1016/j.chemosphere.2021.131766

Duan, C., Ma, T., Wang, J., Zhou, Y., 2020. Removal of heavy metals from aqueous solution using carbon-based adsorbents: A review. J. Water Process Eng. 37, 101339. https://doi.org/10.1016/J.JWPE.2020.101339

El-Naggar, M.E., Wassel, A.R., Shoueir, K., 2021. Visible-light driven photocatalytic effectiveness for solid-state synthesis of ZnO/natural clay/TiO2 nanoarchitectures towards complete decolorization of methylene blue from aqueous solution. Environ.

Nanotechnology, Monit. Manag. 15, 100425. https://doi.org/10.1016/J.ENMM.2020.100425
El Khomri, M., El Messaoudi, N., Dbik, A., Bentahar, S., Fernine, Y., Lacherai, A., Jada, A., 2022a. Optimization Based on Response Surface Methodology of Anionic Dye Desorption From Two Agricultural Solid Wastes. Chem. Africa 5, 1083–1095. https://doi.org/10.1007/S42250-022-00395-4/METRICS
El Khomri, M., El Messaoudi, N., Dbik, A., Bentahar, S., Lacherai, A., Chegini, Z.G., Bouich, A., 2022b. Removal of Congo red from aqueous solution in single and binary mixture systems using Argan nutshell wood. Pigment Resin Technol. 51, 477–488. https://doi.org/10.1108/PRT-04-2021-0045/FULL/XML
El Khomri, M., El Messaoudi, N., Dbik, A., Bentahar, S., Lacherai, A., Faska, N., Jada, A., 2021. Regeneration of argan nutshell and almond shell using HNO3 for their reusability to remove cationic dye from aqueous solution. https://doi.org/10.1080/00986445.2021.1963960 209, 1304–1315. https://doi.org/10.1080/00986445.2021.1963960
El Messaoudi, N., El Khomri, M., Chegini, Z.G., Bouich, A., Dbik, A., Bentahar, S., Labjar, N., Iqbal, M., Jada, A., Lacherai, A., 2021. Dye removal from aqueous solution using nanocomposite synthesized from oxalic acid-modified agricultural solid waste and ZnFe2O4 nanoparticles. Nanotechnol. Environ. Eng. 2021 73 7, 797–811. https://doi.org/10.1007/S41204-021-00173-6
El Messaoudi, N., El Khomri, M., Chegini, Z.G., Dbik, A., Bentahar, S., Iqbal, M., Jada, A., Lacherai, A., 2022a. Desorption of crystal violet from alkali-treated agricultural material waste: an experimental study, kinetic, equilibrium and thermodynamic modeling. Pigment Resin Technol. 51, 309–319. https://doi.org/10.1108/PRT-02-2021-0019/FULL/XML
El Messaoudi, N., El Khomri, M., El Mouden, A., Bouich, A., Jada, A., Lacherai, A., Iqbal, H.M.N., Mulla, S.I., Kumar, V., Américo-Pinheiro, J.H.P., 2022b. Regeneration and reusability of non-conventional low-cost adsorbents to remove dyes from wastewaters in multiple consecutive adsorption–desorption cycles: a review. Biomass Convers. Biorefinery 2022 1–18. https://doi.org/10.1007/S13399-022-03604-9
El Messaoudi, N., El Khomri, M., Fernine, Y., Bouich, A., Lacherai, A., Jada, A., Sher, F., Lima, E.C., 2022c. Hydrothermally engineered Eriobotrya japonica leaves/MgO nanocomposites with potential applications in wastewater treatment. Groundw. Sustain. Dev. 16, 100728. https://doi.org/10.1016/J.GSD.2022.100728
El Messaoudi, N., El Mouden, A., Fernine, Y., El Khomri, M., Bouich, A., Faska, N., Ciğeroğlu, Z., Américo-Pinheiro, J.H.P., Jada, A., Lacherai, A., 2022d. Green synthesis of Ag2O nanoparticles using Punica granatum leaf extract for sulfamethoxazole antibiotic adsorption: characterization, experimental study, modeling, and DFT calculation. Environ. Sci. Pollut. Res. 2022 1–18. https://doi.org/10.1007/S11356-022-21554-7
El Mouden, A., El Guerraf, A., El Messaoudi, N., Haounati, R., Ait El Fakir, A., Lacherai, A., 2022. Date Stone Functionalized with 3-Aminopropyltriethoxysilane as a Potential Biosorbent for Heavy Metal Ions Removal from Aqueous Solution. Chem. Africa. https://doi.org/10.1007/s42250-022-00350-3
Elfeghe, S., Anwar, S., Zhang, Y., 2022. Adsorption and removal studies of cadmium ion onto sulphonic/phosphonic acid functionalization resins. Can. J. Chem. Eng. 100, 3006–3014. https://doi.org/10.1002/CJCE.24400
Es-said, A., Nafai, H., Lamzougui, G., Bouhaouss, A., Bchitou, R., 2021. Comparative adsorption studies of cadmium ions on phosphogypsum and natural clay. Sci. African 13. https://doi.org/10.1016/j.sciaf.2021.e00960
Espart, A., Artime, S., Tort-Nasarre, G., Yara-Varón, E., 2018. Cadmium exposure during

pregnancy and lactation: materno-fetal and newborn repercussions of Cd(II), and Cd–metallothionein complexes. Metallomics 10, 1359–1367. https://doi.org/10.1039/C8MT00174J

Esvandi, Z., Foroutan, R., Mirjalili, M., Sorial, G.A., Ramavandi, B., 2019. Physicochemical Behavior of Penaeuse semisulcatuse Chitin for Pb and Cd Removal from Aqueous Environment. J. Polym. Environ. 27, 263–274. https://doi.org/10.1007/S10924-018-1345-X/FIGURES/12

Foroutan, R., Mohammadi, R., Ahmadi, A., Bikhabar, G., Babaei, F., Ramavandi, B., 2022a. Impact of ZnO and Fe3O4 magnetic nanoscale on the methyl violet 2B removal efficiency of the activated carbon oak wood. Chemosphere 286, 131632. https://doi.org/10.1016/J.CHEMOSPHERE.2021.131632

Foroutan, R., Mohammadi, R., Ramavandi, B., Bastanian, M., 2018. Removal characteristics of chromium by activated carbon/CoFe 2 O 4 magnetic composite and Phoenix dactylifera stone carbon. Korean J. Chem. Eng 35, 2207–2219. https://doi.org/10.1007/s11814-018-0145-2

Foroutan, R., Peighambardoust, S.J., Aghdasinia, H., Mohammadi, R., Ramavandi, B., 2020. Modification of bio-hydroxyapatite generated from waste poultry bone with MgO for purifying methyl violet-laden liquids. Environ. Sci. Pollut. Res. 27, 44218–44229. https://doi.org/10.1007/S11356-020-10330-0/TABLES/1

Foroutan, R., Peighambardoust, S.J., Hemmati, S., Ahmadi, A., Falletta, E., Ramavandi, B., Bianchi, C.L., 2021a. Zn2+ removal from the aqueous environment using a polydopamine/hydroxyapatite/Fe3O4 magnetic composite under ultrasonic waves. RSC Adv. 11, 27309–27321. https://doi.org/10.1039/D1RA04583K

Foroutan, R., Peighambardoust, S.J., Hemmati, S., Khatooni, H., Ramavandi, B., 2021b. Preparation of clinoptilolite/starch/CoFe2O4 magnetic nanocomposite powder and its elimination properties for cationic dyes from water and wastewater. Int. J. Biol. Macromol. 189, 432–442. https://doi.org/10.1016/J.IJBIOMAC.2021.08.144

Foroutan, R., Peighambardoust, S.J., Mohammadi, R., Peighambardoust, S.H., Ramavandi, B., 2022b. Development of new magnetic adsorbent of walnut shell ash/starch/Fe3O4 for effective copper ions removal: Treatment of groundwater samples. Chemosphere 296, 133978. https://doi.org/10.1016/J.CHEMOSPHERE.2022.133978

Foroutan, R., Peighambardoust, S.J., Mohammadi, R., Peighambardoust, S.H., Ramavandi, B., 2022c. Cadmium ion removal from aqueous media using banana peel biochar/Fe3O4/ZIF-67. Environ. Res. 211, 113020. https://doi.org/10.1016/J.ENVRES.2022.113020

Guo, L., Zhang, S.T., Li, W.P., Hu, G., Li, X., 2014. Experimental and computational studies of two antibacterial drugs as corrosion inhibitors for mild steel in acid media. Mater. Corros. 65, 935–942. https://doi.org/10.1002/maco.201307346

Haounati, R., Ouachtak, H., El Haouti, R., Akhouairi, S., Largo, F., Akbal, F., Benlhachemi, A., Jada, A., Addi, A.A., 2021. Elaboration and properties of a new SDS/CTAB@Montmorillonite organoclay composite as a superb adsorbent for the removal of malachite green from aqueous solutions. Sep. Purif. Technol. 255. https://doi.org/10.1016/j.seppur.2020.117335

Hsissou, R., Benzidia, B., Rehioui, M., Berradi, M., Berisha, A., Assouag, M., Hajjaji, N., Elharfi, A., 2019. Anticorrosive property of hexafunctional epoxy polymer HGTMDAE for E24 carbon steel corrosion in 1.0 M HCl: gravimetric, electrochemical, surface morphology and molecular dynamic simulations. Polym. Bull. 2019 777 77, 3577–3601. https://doi.org/10.1007/S00289-019-02934-5

Irawan, C., Nata, I.F., Lee, C.K., 2019. Removal of Pb(II) and As(V) using magnetic nanoparticles coated montmorillonite via one-pot solvothermal reaction as adsorbent. J. Environ. Chem. Eng. 7. https://doi.org/10.1016/j.jece.2019.103000

Isiuku, B.O., Enyoh, C.E., Duru, C.E., Ibe, F.C., 2021. Phosphate ions removal from aqueous phase by batch adsorption on activated (activation before carbonization) biochar derived from rubber pod husk. Curr. Res. Green Sustain. Chem. 4, 100136. https://doi.org/10.1016/J.CRGSC.2021.100136

Jafari, H., Ameri, E., Rezaeivala, M., Berisha, A., Halili, J., 2022. Anti-corrosion behavior of two N2O4 Schiff-base ligands: Experimental and theoretical studies. J. Phys. Chem. Solids 164, 110645. https://doi.org/10.1016/J.JPCS.2022.110645

Jamshidiyan, M., Shirani, A.S., Alahyarizadeh, G., 2017. Solvothermal synthesis and characterization of magnetic Fe3O4 nanoparticle by different sodium salt sources. Mater. Sci. Pol. 35, 50–57. https://doi.org/10.1515/MSP-2017-0004

Ji, J., Ge, Y., Balsam, W., Damuth, J.E., Chen, J., 2009. Rapid identification of dolomite using a Fourier Transform Infrared Spectrophotometer (FTIR): A fast method for identifying Heinrich events in IODP Site U1308. Mar. Geol. 258, 60–68. https://doi.org/10.1016/J.MARGEO.2008.11.007

Jiang, C., Wang, X., Hou, B., Hao, C., Li, X., Wu, J., 2020. Construction of a Lignosulfonate-Lysine Hydrogel for the Adsorption of Heavy Metal Ions. J. Agric. Food Chem. 68, 3050–3060. https://doi.org/10.1021/acs.jafc.9b07540

Joshi, N.C., Kaur, K., Kumar, N., Bhandari, N.S., Thakur, A., 2021. Synthesis and adsorption applications of PPY/Fe3O4 nanocomposite based material. Nano-Structures & Nano-Objects 25, 100669. https://doi.org/10.1016/j.nanoso.2021.100669

Khalaf, B., Hamed, O., Jodeh, S., Bol, R., Hanbali, G., Safi, Z., Dagdag, O., Berisha, A., Samhan, S., 2021. Cellulose-Based Hectocycle Nanopolymers: Synthesis, Molecular Docking and Adsorption of Difenoconazole from Aqueous Medium. Int. J. Mol. Sci. 2021, Vol. 22, Page 6090 22, 6090. https://doi.org/10.3390/IJMS22116090

Khan, S.A., Khan, T.A., 2021. Clay-hydrogel nanocomposites for adsorptive amputation of environmental contaminants from aqueous phase: A review. J. Environ. Chem. Eng. 9, 105575. https://doi.org/10.1016/J.JECE.2021.105575

Khomri, M. El, Messaoudi, N. El, Dbik, A., Bentahar, S., Fernine, Y., Bouich, A., Lacherai, A., Jada, A., 2022. Modification of low-cost adsorbent prepared from agricultural solid waste for the adsorption and desorption of cationic dye. Emergent Mater. 5, 1679–1688. https://doi.org/10.1007/S42247-022-00390-Y/METRICS

Lima, E.C., Hosseini-Bandegharaei, A., Moreno-Piraján, J.C., Anastopoulos, I., 2019. A critical review of the estimation of the thermodynamic parameters on adsorption equilibria. Wrong use of equilibrium constant in the Van't Hoof equation for calculation of thermodynamic parameters of adsorption. J. Mol. Liq. 273, 425–434. https://doi.org/10.1016/J.MOLLIQ.2018.10.048

Lin, Z., Weng, X., Ma, L., Sarkar, B., Chen, Z., 2019. Mechanistic insights into Pb(II) removal from aqueous solution by green reduced graphene oxide. J. Colloid Interface Sci. 550, 1–9. https://doi.org/10.1016/J.JCIS.2019.04.078

Liu, X. Di, Chen, H., Liu, S.S., Ye, L.Q., Li, Y.P., 2015. Hydrothermal synthesis of superparamagnetic Fe3O4 nanoparticles with ionic liquids as stabilizer. Mater. Res. Bull. 62, 217–221. https://doi.org/10.1016/J.MATERRESBULL.2014.11.022

Liu, S., Yu, B., Wang, S., Shen, Y., Cong, H., 2020. Preparation, surface functionalization and application of Fe3O4 magnetic nanoparticles. Adv. Colloid Interface Sci. 281, 102165. https://doi.org/10.1016/j.cis.2020.102165

Malega, F., Indrayana, I.P.T., Suharyadi, E., 2018. Synthesis and Characterization of the Microstructure and Functional Group Bond of Fe3o4 Nanoparticles from Natural Iron Sand in Tobelo North Halmahera. J. Ilm. Pendidik. Fis. Al-Biruni 7, 129–138. https://doi.org/10.24042/jipfalbiruni.v7i2.2913

Massaro, M., Iborra, C.V., Cavallaro, G., Colletti, C.G., García-villén, F., Lazzara, G., Riela, S., 2021. Synthesis and characterization of nanomaterial based on halloysite and

hectorite clay minerals covalently bridged. Nanomaterials 11, 1–13. https://doi.org/10.3390/nano11020506
Messaoudi, N. El, Mouden, A. El, Khomri, M. El, Bouich, A., Fernine, Y., Ciğeroğlu, Z., Américo-Pinheiro, J.H.P., Labjar, N., Jada, A., Sillanpää, M., Lacherai, A., 2022. Experimental study and theoretical statistical modeling of acid blue 25 remediation using activated carbon from Citrus sinensis leaf. Fluid Phase Equilib. 563, 113585. https://doi.org/10.1016/J.FLUID.2022.113585
Mitra, S., Chakraborty, A.J., Tareq, A.M., Emran, T. Bin, Nainu, F., Khusro, A., Idris, A.M., Khandaker, M.U., Osman, H., Alhumaydhi, F.A., Simal-Gandara, J., 2022. Impact of heavy metals on the environment and human health: Novel therapeutic insights to counter the toxicity. J. King Saud Univ. - Sci. 34, 101865. https://doi.org/10.1016/J.JKSUS.2022.101865
Mohankumar, M., Praveen Kumar, S., Guruprasad, B., Manavalla, S., Isaac Joshuaramesh Lalvani, J.S.C., Somasundaram, P.L., Tamilarasu, P., Tanwar, P.S., 2021. XRD Peak Profile Analysis of SiC Reinforced Al2O3Ceramic Composite Synthesized by Electrical Resistance Heating and Microwave Sintering: A Comparison. Adv. Mater. Sci. Eng. 2021. https://doi.org/10.1155/2021/8341924
Munir, N., Jahangeer, M., Bouyahya, A., Omari, N. El, Ghchime, R., Balahbib, A., Aboulaghras, S., Mahmood, Z., Akram, M., Shah, S.M.A., Mikolaychik, I.N., Derkho, M., Rebezov, M., Venkidasamy, B., Thiruvengadam, M., Shariati, M.A., 2021. Heavy Metal Contamination of Natural Foods Is a Serious Health Issue: A Review. Sustain. 2022, Vol. 14, Page 161 14, 161. https://doi.org/10.3390/SU14010161
Nairat, N., Hamed, O., Berisha, A., Jodeh, S., Algarra, M., Azzaoui, K., Dagdag, O., Samhan, S., 2022. Cellulose polymers with β-amino ester pendant group: design, synthesis, molecular docking and application in adsorption of toxic metals from wastewater. BMC Chem. 16, 1–21. https://doi.org/10.1186/S13065-022-00837-7/TABLES/5
Pehlivan, E., Özkan, A.M., Dinç, S., Parlayici, Ş., 2009. Adsorption of Cu2+ and Pb2+ ion on dolomite powder. J. Hazard. Mater. 167, 1044–1049. https://doi.org/10.1016/j.jhazmat.2009.01.096
Peighambardoust, S.J., Foroutan, R., Peighambardoust, S.H., Khatooni, H., Ramavandi, B., 2021. Decoration of Citrus limon wood carbon with Fe3O4 to enhanced Cd2+ removal: A reclaimable and magnetic nanocomposite. Chemosphere 282, 131088. https://doi.org/10.1016/J.CHEMOSPHERE.2021.131088
Polidori, E., 2007. Relationship Between the Atterberg Limits and Clay Content. Soils Found. 47, 887–896. https://doi.org/10.3208/SANDF.47.887
Qiu, G., Xie, Q., Liu, H., Chen, T., Xie, J., Li, H., 2015. Removal of Cu(II) from aqueous solutions using dolomite-palygorskite clay: Performance and mechanisms. Appl. Clay Sci. 118, 107–115. https://doi.org/10.1016/J.CLAY.2015.09.008
Rappé, A.K., Casewit, C.J., Colwell, K.S., Goddard, W.A., Skiff, W.M., 1992. UFF, a Full Periodic Table Force Field for Molecular Mechanics and Molecular Dynamics Simulations. J. Am. Chem. Soc. 114, 10024–10035. https://doi.org/10.1021/JA00051A040/SUPPL_FILE/JA00051A040_SI_001.PDF
Rezaei Kalantry, R., Jafari, A.J., Esrafili, A., Kakavandi, B., Gholizadeh, A., Azari, A., 2015. Optimization and evaluation of reactive dye adsorption on magnetic composite of activated carbon and iron oxide. New pub Balaban 57, 6411–6422. https://doi.org/10.1080/19443994.2015.1011705
Sen Gupta, S., Bhattacharyya, K.G., 2008. Immobilization of Pb(II), Cd(II) and Ni(II) ions on kaolinite and montmorillonite surfaces from aqueous medium. J. Environ. Manage. 87, 46–58. https://doi.org/10.1016/J.JENVMAN.2007.01.048
Sharma, M., Singh, J., Hazra, S., Basu, S., 2019. Adsorption of heavy metal ions by mesoporous ZnO and TiO2@ZnO monoliths: Adsorption and kinetic studies.

Microchem. J. 145, 105–112. https://doi.org/10.1016/J.MICROC.2018.10.026
Shrestha, R., Ban, S., Devkota, S., Sharma, S., Joshi, R., Tiwari, A.P., Kim, H.Y., Joshi, M.K., 2021. Technological trends in heavy metals removal from industrial wastewater: A review. J. Environ. Chem. Eng. 9, 105688. https://doi.org/10.1016/J.JECE.2021.105688
Şimşek, S., Şenol, Z.M., Ulusoy, H.İ., 2017. Synthesis and characterization of a composite polymeric material including chelating agent for adsorption of uranyl ions. J. Hazard. Mater. 338, 437–446. https://doi.org/10.1016/J.JHAZMAT.2017.05.059
Srivastava, N.K., Majumder, C.B., 2008. Novel biofiltration methods for the treatment of heavy metals from industrial wastewater. J. Hazard. Mater. 151, 1–8. https://doi.org/10.1016/J.JHAZMAT.2007.09.101
Szabó, T., Bakandritsos, A., Tzitzios, V., Papp, S., Korösi, L., Galbács, G., Musabekov, K., Bolatova, D., Petridis, D., Dékány, I., 2007. Magnetic iron oxide/clay composites: effect of the layer silicate support on themicrostructure and phase formation of magnetic nanoparticles. Nanotechnology 18, 285602. https://doi.org/10.1088/0957-4484/18/28/285602
Tadjarodi, A., Abbaszadeh, A., Taghizadeh, M., Shekari, N., Asgharinezhad, A.A., 2015. Solid phase extraction of Cd(II) and Pb(II) ions based on a novel functionalized Fe3O4@ SiO2 core-shell nanoparticles with the aid of multivariate optimization methodology. Mater. Sci. Eng. C 49, 416–421. https://doi.org/10.1016/J.MSEC.2015.01.013
Tan, K.L., Hameed, B.H., 2017. Insight into the adsorption kinetics models for the removal of contaminants from aqueous solutions. J. Taiwan Inst. Chem. Eng. 74, 25–48. https://doi.org/10.1016/J.JTICE.2017.01.024
Tan, Z., Wang, Y., Kasiulienė, A., Huang, C., Ai, P., 2017. Cadmium removal potential by rice straw-derived magnetic biochar. Clean Technol. Environ. Policy 19, 761–774. https://doi.org/10.1007/s10098-016-1264-2
Ulusoy, S., B Akalin, R., Çevikbaş, H., Berisha, A., Oral, A., Boşgelmez-Tinaz, G., 2022. Zeolite 4A as a jammer of bacterial communication in Chromobacterium violaceum and Pseudomonas aeruginosa. Future Microbiol. 17. https://doi.org/10.2217/FMB-2021-0174
Van Tran, T., Nguyen, D.T.C., Le, H.T.N., Bach, L.G., Vo, D.V.N., Lim, K.T., Nong, L.X., Nguyen, T.D., 2019. Combined Minimum-Run Resolution IV and Central Composite Design for Optimized Removal of the Tetracycline Drug Over Metal–Organic Framework-Templated Porous Carbon. Mol. 2019, Vol. 24, Page 1887 24, 1887. https://doi.org/10.3390/MOLECULES24101887
Wan Fatihah Khairunisa Wan Nor, S., Kamilah Che Soh, S., Azzura Abd Rahman Azmi, A., Sukeri Mohd Yusof, M., Shamsuddin, M., 2018. SYNTHESIS AND PHYSICOCHEMICAL PROPERTIES OF MAGNETITE NANOPARTICLES (Fe3O4) AS POTENTIAL SOLID SUPPORT FOR HOMOGENEOUS CATALYSTS. Malaysian J. Anal. Sci. 22, 768–774. https://doi.org/10.17576/mjas-2018-2205-04
Wang, N., Yang, D., Wang, X., Yu, S., Wang, H., Wen, T., Song, G., Yu, Z., Wang, X., 2018. Highly efficient Pb(ii) and Cu(ii) removal using hollow Fe 3 O 4 @PDA nanoparticles with excellent application capability and reusability. Inorg. Chem. Front. 5, 2174–2182. https://doi.org/10.1039/C8QI00541A
Wang, S., Gainey, L., Baxter, D., Wang, X., Mackinnon, I.D.R., Xi, Y., 2021. Thermal behaviours of clay mixtures during brick firing: A combined study of in-situ XRD, TGA and thermal dilatometry. Constr. Build. Mater. 299, 124319. https://doi.org/10.1016/j.conbuildmat.2021.124319
Xu, M., Zhang, Y., Zhang, Z., Shen, Y., Zhao, M., Pan, G., 2011. Study on the adsorption of Ca2+, Cd2+ and Pb2+ by magnetic Fe3O4 yeast treated with EDTA dianhydride. Chem. Eng. J. 168, 737–745. https://doi.org/10.1016/J.CEJ.2011.01.069
Xu, Z.L., Zhang, B., Gang, Y., Cao, K., Garakani, M.A., Abouali, S., Huang, J., Huang, J.Q., Heidari, E.K., Wang, H., Kim, J.K., 2015. In-situ TEM examination and exceptional

long-term cyclic stability of ultrafine Fe3O4 nanocrystal/carbon nanofiber composite electrodes. Energy Storage Mater. 1, 25–34. https://doi.org/10.1016/J.ENSM.2015.08.002

Yang, D., Song, S., Zou, Y., Wang, X., Yu, S., Wen, T., Wang, H., Hayat, T., Alsaedi, A., Wang, X., 2017. Rational design and synthesis of monodispersed hierarchical SiO2@layered double hydroxide nanocomposites for efficient removal of pollutants from aqueous solution. Chem. Eng. J. 323, 143–152. https://doi.org/10.1016/J.CEJ.2017.03.158

Yang, D., Wang, X., Wang, N., Zhao, G., Song, G., Chen, D., Liang, Y., Wen, T., Wang, H., Hayat, T., Alsaedi, A., Wang, X., Wang, S., 2018. In-situ growth of hierarchical layered double hydroxide on polydopamine-encapsulated hollow Fe3O4 microspheres for efficient removal and recovery of U(VI). J. Clean. Prod. 172, 2033–2044. https://doi.org/10.1016/J.JCLEPRO.2017.11.219

Yang, K., Peng, H., Wen, Y., Li, N., 2010. Re-examination of characteristic FTIR spectrum of secondary layer in bilayer oleic acid-coated Fe3O4 nanoparticles. Appl. Surf. Sci. 256, 3093–3097. https://doi.org/10.1016/J.APSUSC.2009.11.079

Yang, W., Luo, W., Sun, T., Xu, Y., Sun, Y., 2022. Adsorption Performance of Cd(II) by Chitosan-Fe3 O4-Modified Fish Bone Char. Int. J. Environ. Res. Public Health 19. https://doi.org/10.3390/IJERPH19031260

Yeow, P., … S.W.-… R. in A., 2021, undefined, 2021. Removal of azo and anthraquinone dye by plant biomass as adsorbent—a review. biointerfaceresearch.com 11, 8218–8232. https://doi.org/10.33263/BRIAC111.82188232

Zhang, Z., Wang, T., Zhang, H., Liu, Y., Xing, B., 2021. Adsorption of Pb(II) and Cd(II) by magnetic activated carbon and its mechanism. Sci. Total Environ. 757, 143910. https://doi.org/10.1016/J.SCITOTENV.2020.143910

Zhu, M., Zhu, L., Wang, J., Yue, T., Li, R., Li, Z., 2017. Adsorption of Cd(II) and Pb(II) by in situ oxidized Fe3O4 membrane grafted on 316L porous stainless steel filter tube and its potential application for drinking water treatment. J. Environ. Manage. 196, 127–136. https://doi.org/10.1016/J.JENVMAN.2017.02.073

Zyoud, A.H., Zubi, A., Zyoud, S.H., Hilal, M.H., Zyoud, S., Qamhieh, N., Hajamohideen, A.R., Hilal, H.S., 2019. Kaolin-supported ZnO nanoparticle catalysts in self-sensitized tetracycline photodegradation: Zero-point charge and pH effects. Appl. Clay Sci. 182, 105294. https://doi.org/10.1016/J.CLAY.2019.105294

Figures List

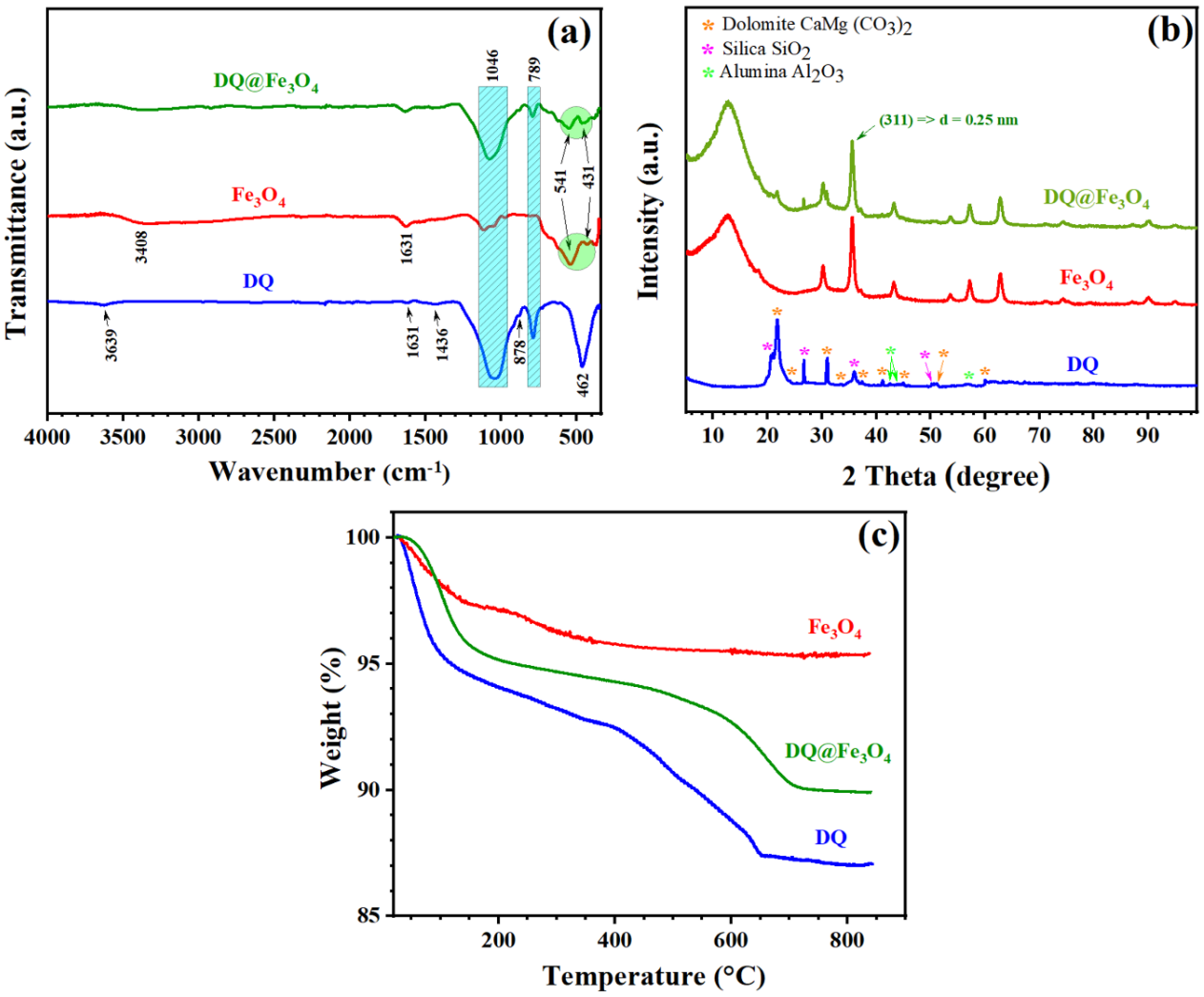

Fig. 1. FTIR spectra (**a**), XRD patterns (**b**), and TGA curves (**c**) of DQ, Fe_3O_4, and DQ@Fe_3O_4.

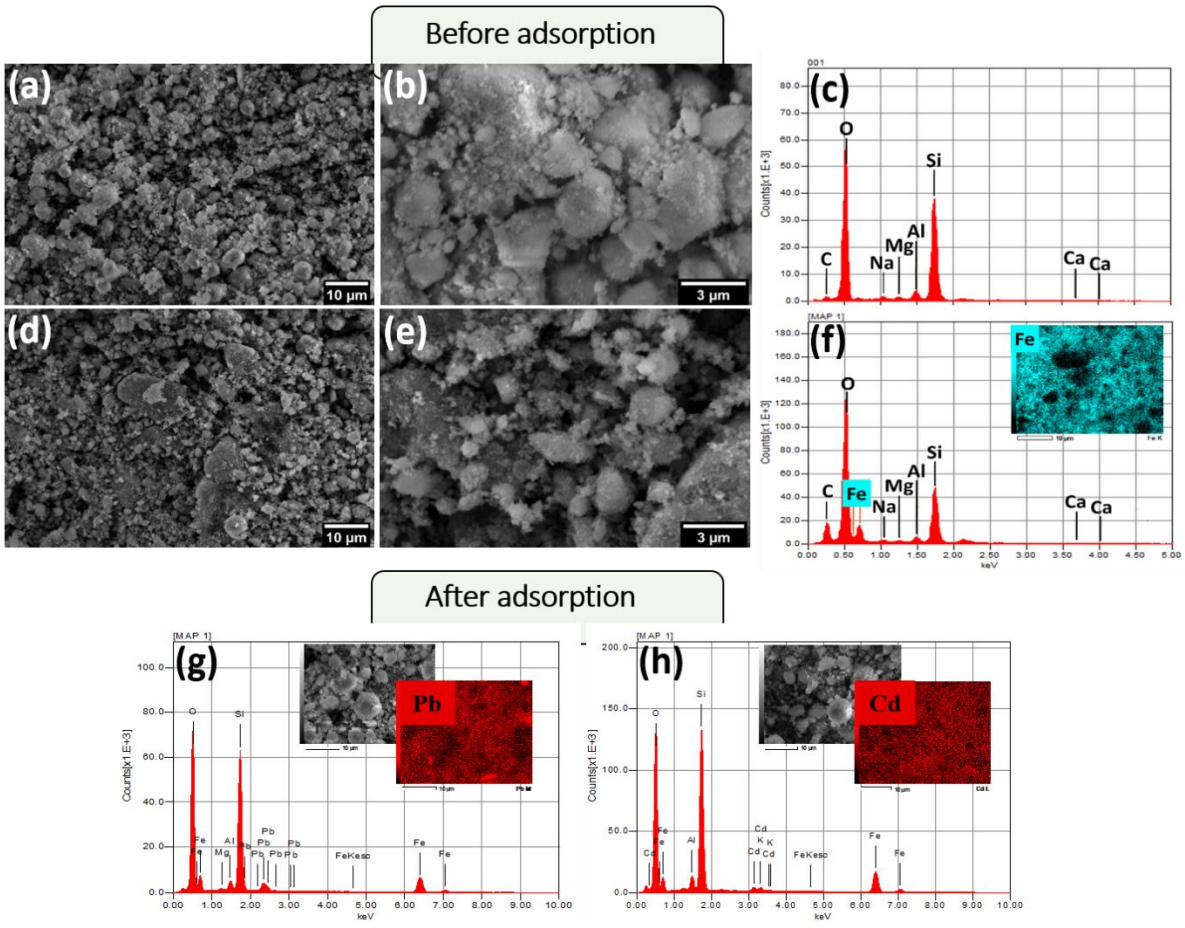

Fig. 2. SEM micrographs and the corresponding EDS spectra of DQ (**a, b, c**), and DQ@Fe_3O_4 (**d, e, f**), and EDS spectra of DQ@Fe_3O_4 after adsorption of Pb^{2+} (**g**) and Cd^{2+} (**h**) ions.

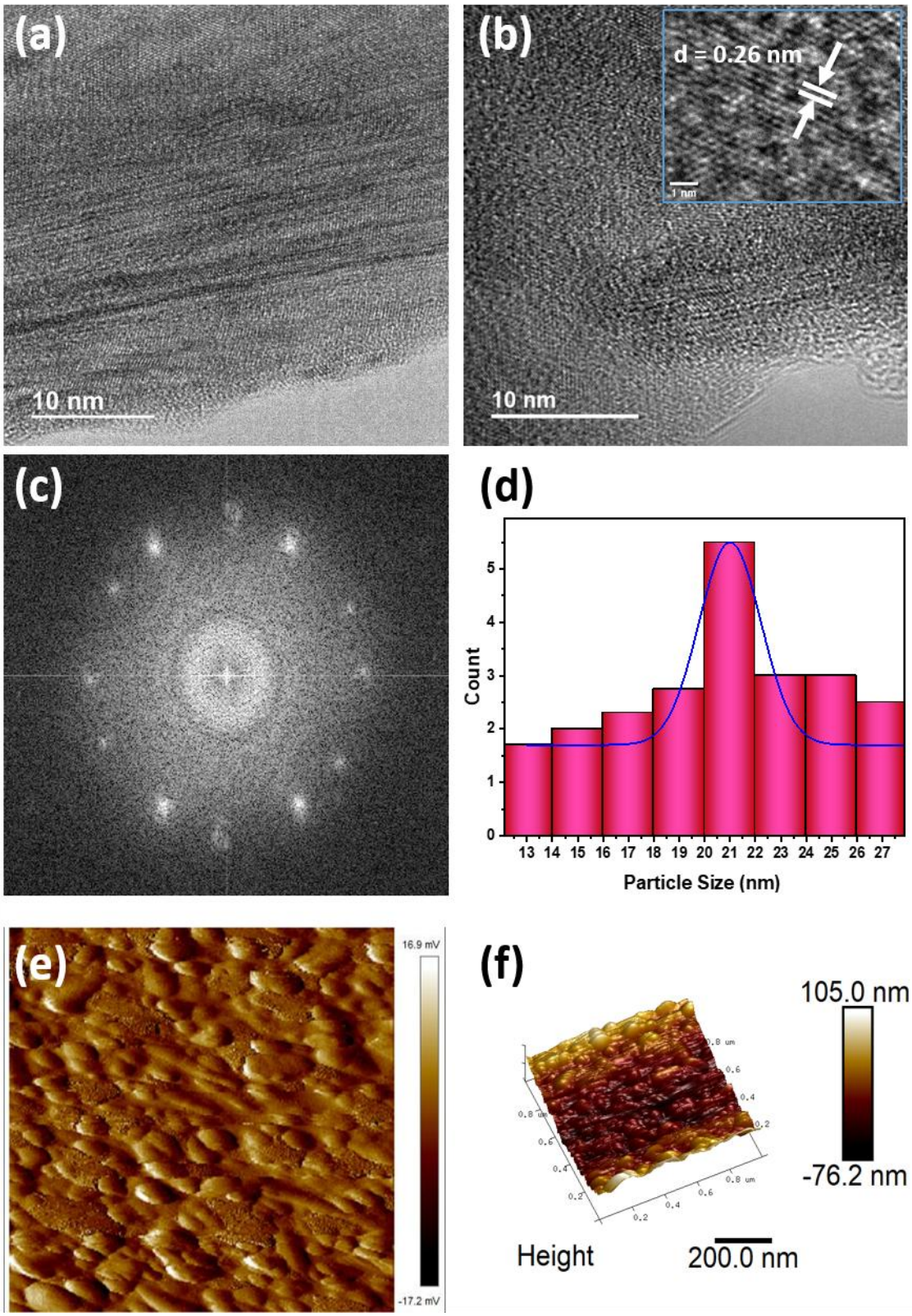

Fig. 3. TEM micrographs (**a, b**), corresponding SAED patterns (**c**), size particle (d), and AFM images (**e, f**) of DQ@Fe_3O_4 nanocomposite.

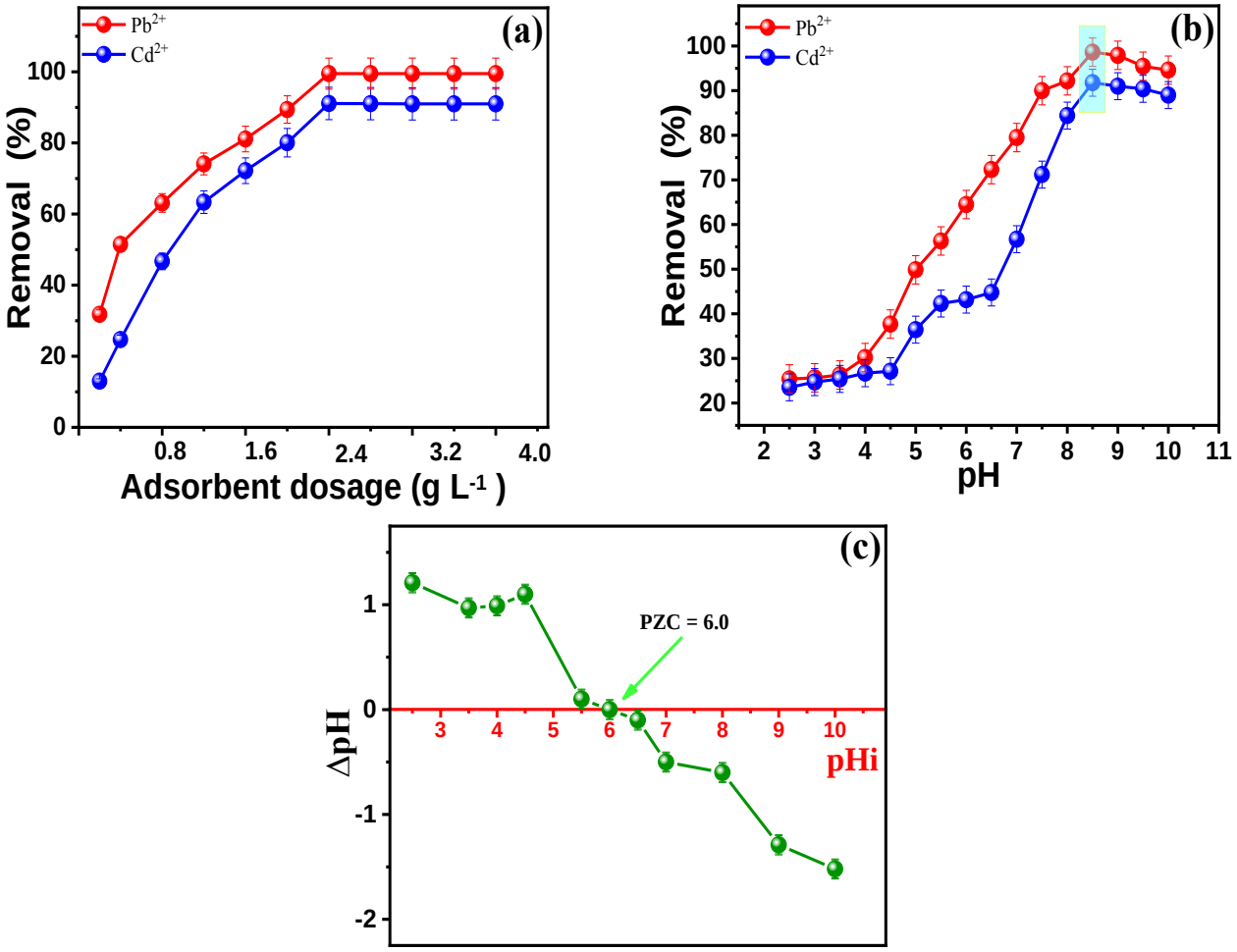

Fig. 4. Effect of adsorbent dosage (**a**) and initial solution pH (**b**) on the adsorption of Pb^{2+} and Cd^{2+} ions, and PZC of DQ@Fe_3O_4 nanocomposite (**c**).

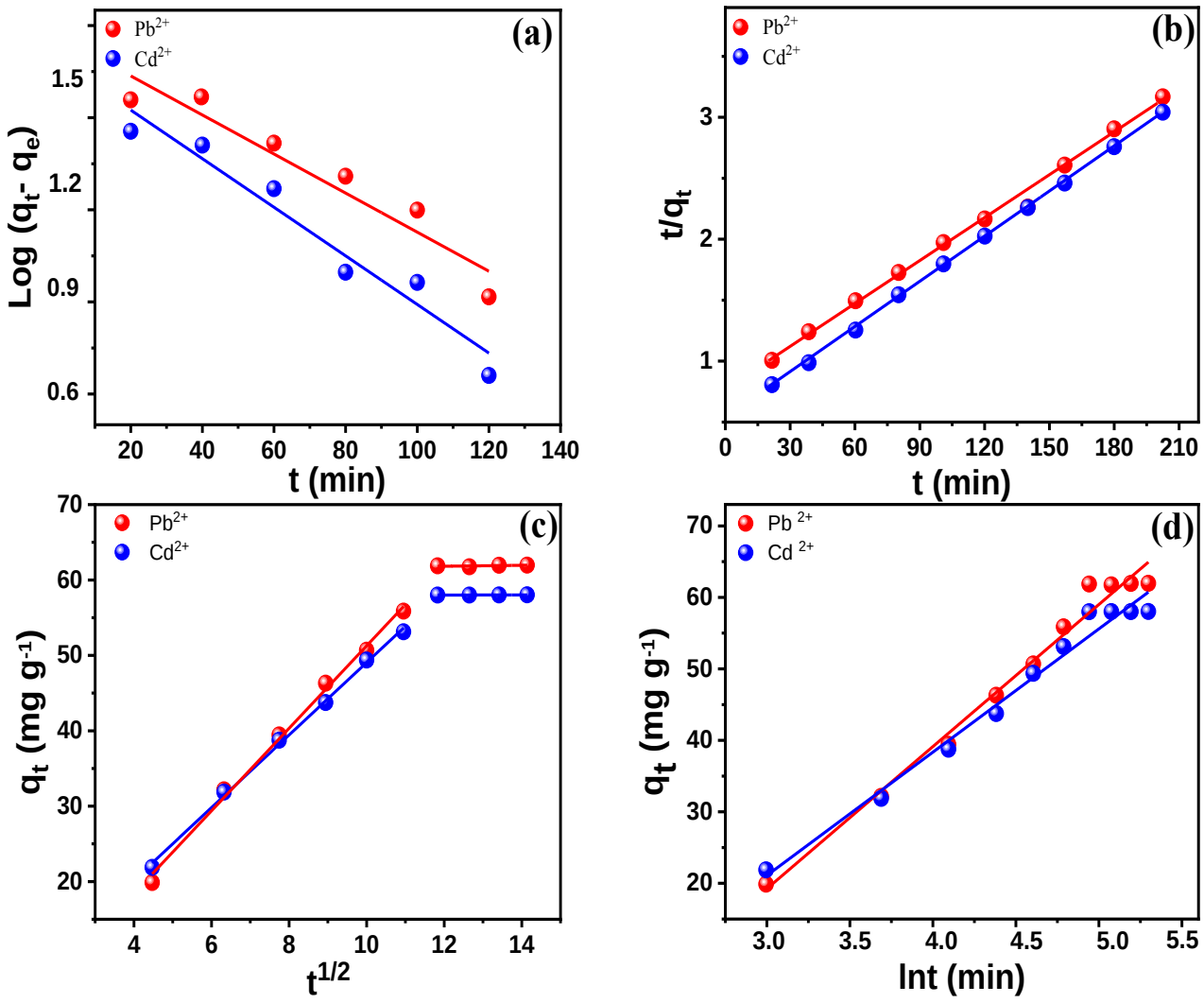

Fig. 5. Linear fitting with the PFO (**a**), the PSO (**b**), IPD (**c**), and the Elovich (**d**) kinetic models of Pb^{2+} and Cd^{2+} adsorption onto DQ@Fe_3O_4 nancomposite.

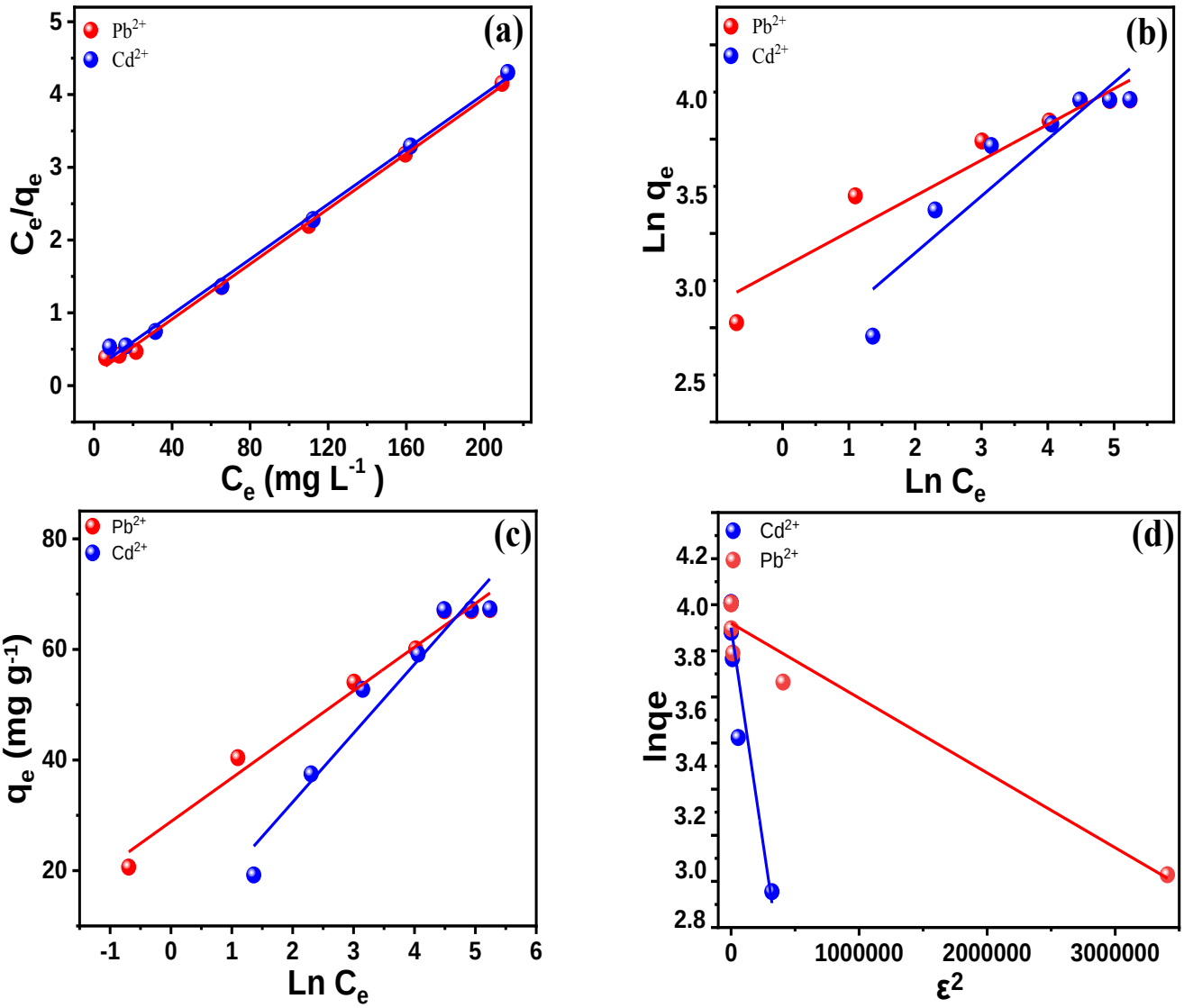

Fig. 6. Langmuir (**a**), Freundlich (**b**), Temkin (**c**), and Dubinin-Radushkevich (**d**) isotherm models for Pb^{2+} and Cd^{2+} adsorption onto DQ@Fe_3O_4 nancomposite.

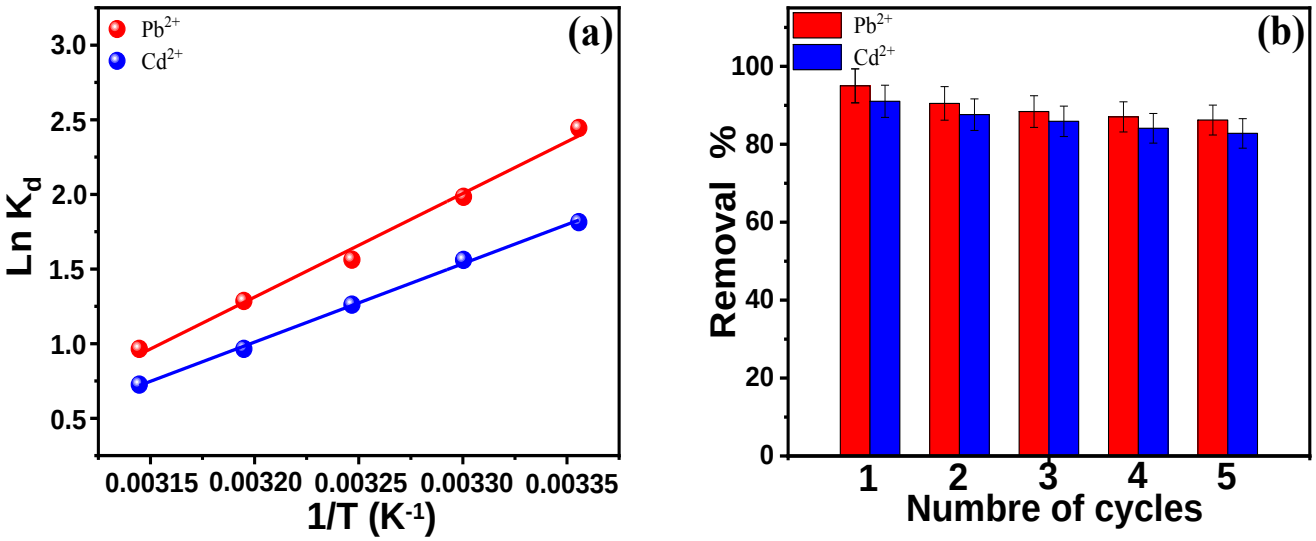

Fig. 7. Plots $\ln K_d$ against 1/T for thermodynamic parameters calculation (**a**) and reusability of DQ@Fe_3O_4 for the Pb^{2+} and Cd^{2+} ions removal (**b**).

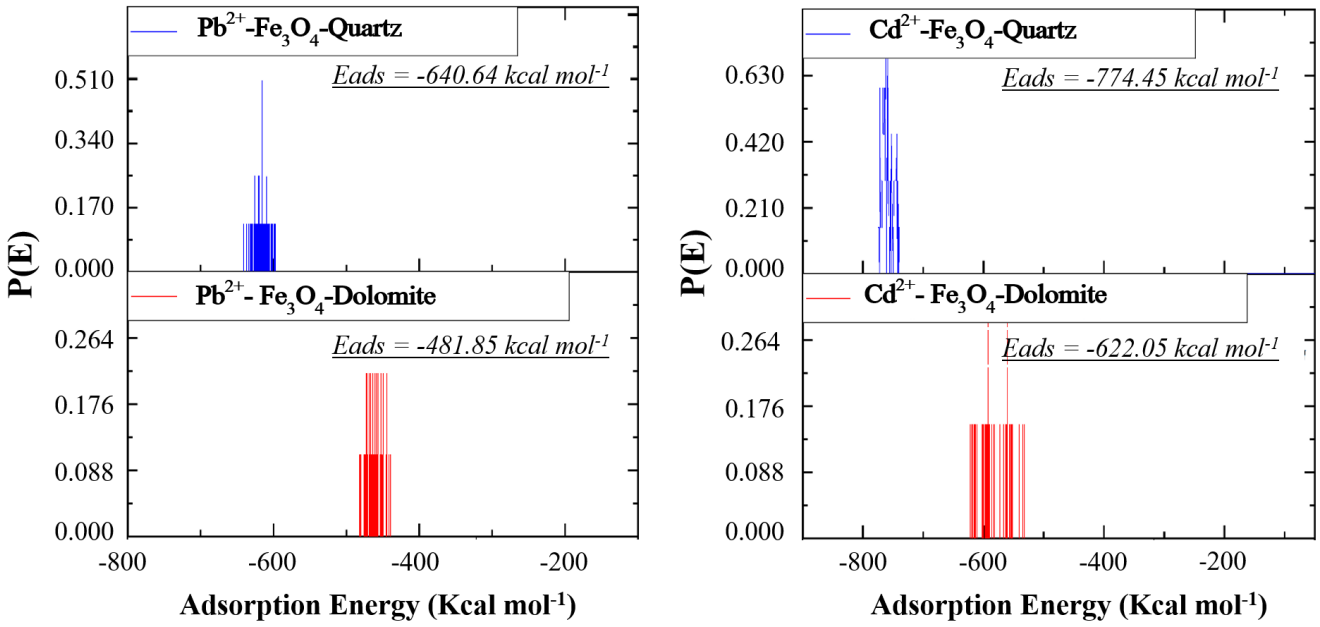

Fig. 8. Probability of the adsorption energy distributions during MC for the $Pb^{2+}$and Cd^{2+} ions on the modeled surfaces of dolomite-Fe_3O_4 and quartz-Fe_3O_4 surface.

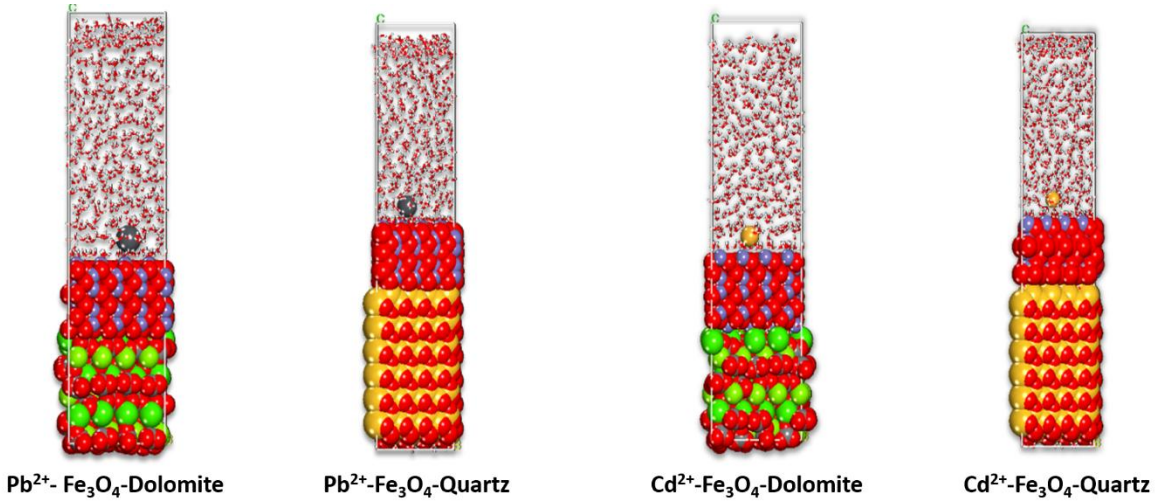

Fig. 9. Geometry of the Lowest energy poses obtained after MC for the Pb^{2+} and Cd^{2+} ions on the modeled surfaces of dolomite-Fe_3O_4 and quartz-Fe_3O_4 surface.

Tables

Table 1. Kinetic parameters of Pb^{2+} and Cd^{2+} adsorption on $DQ@Fe_3O_4$ nancomposite.

Model	**Parameter**	**$DQ@Fe_3O_4$**	
		Pb^{2+}	**Cd^{2+}**
	$q_{e,exp}$ (mg g^{-1})	61.96	58.08
PFO	$q_{e,PFO}$ (mg g^{-1})	48.79	43.69
$Log(q_e - q_t) = Log(q_e) - \frac{K_{PFO}}{2.303}t$	K_{PFO} (min^{-1})	0.017	0.018
	R^2	0.862	0.818
PSO	$q_{e,PSO}$ (mg g^{-1})	63.92	60.19
$\frac{t}{q_t} = \frac{1}{K_{PSO}{q_e}^2} + \frac{1}{q_e}t$	K_{PSO} (g mg^{-1} min^{-1})	0.001	0.002
	R^2	0.999	0.998
IPD	K_{IPD} (mg g^{-1} $min^{-1/2}$)	0.010	0.034
$q_t = K_{IDP}t^{1/2} + C$	C (mg g^{-1})	57.87	33.57
	R^2	0.934	0.907
Elovich	α (mg g^{-1} min^{-1})	2.605	2.917
$q_t = \frac{1}{\beta}\ln(\alpha\beta) + \frac{1}{\beta}lnt$	β (g mg^{-1})	0.050	0.057
	R^2	0.983	0.981

Table 2. Isotherm parameters of Pb^{2+} and Cd^{2+} adsorption on DQ@Fe_3O_4 nancomposite.

Model	**Parameter**	**DQ@Fe_3O_4**	
		Pb^{2+}	**Cd^{2+}**
Langmuir	Q_m (mg g^{-1})	71.42	68.49
$\frac{C_e}{q_e} = \frac{1}{K_L Q_m} + \frac{C_e}{Q_m}$	K_L (L mg^{-1})	0.289	0.109
	R_L	0.023	0.058
	R^2	0.999	0.999
Freundlich	K_F (mg g^{-1})	26.65	16.34
$Lnq_e = LnK_F + \frac{LnC_e}{n_F}$	$1/n_F$	0.189	0.301
	R^2	0.928	0.868
Temkin	b_T (kJ mol^{-1})	0.314	0.198
$q_e = \frac{RT}{b_T} LnK_T + \frac{RT}{b_T} LnC_e$	K_T (L mg^{-1})	38.85	1.819
	R^2	0.981	0.944
Dubinin-Radushkevich	Q_m (mg g^{-1})	59.34	60.406
$Lnq_e = LnQ_m - \beta\varepsilon^2$	E (kJ mol^{-1})	2.236	0.353
	R^2	0.957	0.907

Table 3. Comparison of $Pb^{2+}$and Cd^{2+} removal of DQ@Fe_3O_4 nancomposite with other adsorbents.

Adsorbent	**Q_m (mg g^{-1})**		**Reference**
	Pb^{2+}	**Cd^{2+}**	
DQ@Fe_3O_4	71.42	68.49	Current study
DS@APTS	11.68	-	(El Mouden et al., 2022)
Purometᵀᴹ MTS9570	-	51.02	(Elfeghe et al., 2022)
BPB/Fe_3O_4/ZIF-67	-	50.78	(Foroutan et al., 2022c)
BPB/Fe_3O_4	-	30.33	(Foroutan et al., 2022c)
HDTMA-bentonite	25.80	-	(Dinh et al., 2022)
PPy/Fe_3O_4	11.35	8.92	(Joshi et al., 2021)
Mt@MH	38.15	-	(Irawan et al., 2019)
Fe_3O_4@PDA	57.25	-	(Wang et al., 2018)
Fe_3O_4 membranes	2.25	0.8	(Zhu et al., 2017)
Fe_3O_4@SiO_2 core-shell	156	179	(Tadjarodi et al., 2015)
Fe_3O_4/cyclodextrin	64.5	27.7	(Badruddoza et al., 2013)
Blast furnace slug	40.00	38.00	(Ahmaruzzaman, 2011)
EDTAD-Fe_3O_4	99.26	48.7	(Xu et al., 2011)
Dolomite powder	21.74	-	(Pehlivan et al., 2009)
Kaolinite	11.5	6.8	(Sen Gupta and Bhattacharyya, 2008)
montmorillonite	31.1	30.7	(Sen Gupta and Bhattacharyya, 2008)

Table 4. Sorption thermodynamic parameters of $Pb^{2+}$and Cd^{2+} on DQ@Fe_3O_4 at different temperatures.

Metal	***T* (K)**	***ΔG*° (kJ mol^{-1})**	***ΔH*° (kJ mol^{-1})**	***ΔS*° (J mol^{-1} K^{-1})**
	298	-07.291		
	303	-06 .254		
Pb^{2+}	308	-05.278	–57.740	–169.713
	313	-04.644		
	318	-03.869		
	298	-05 .729		
	303	-05 .188		
Pb^{2+}	308	-04 .506	–43.688	–127.245
	313	-03.808		
	318	-03.238		